International Journal of Mathematical, Engineering and Management Sciences
Vol. 10, No. 3, 676-703, 2025
https://doi.org/10.33889/IJMEMS.2025.10.3.035

Ram Arti Publishers

Mathematical Study of Dispersion of Nano Biosensors in an Artery with Multiple Stenosis

Bhawini Prasad
Department of Mathematics,
Harcourt Butler Technical University, Kanpur, 208002, Uttar Pradesh, India.
E-mail: jayabhawini@gmail.com

(Received on July 18, 2024; Revised on October 1, 2024 & November 23, 2024 & December 14, 2024;
Accepted on December 20, 2024)

Abstract
This research article deals with the usefulness of nanobiosensors to treat multiple stenosis in an artery. Nanobiosensors dispersed in blood are recognised as nanofluids, and their properties have been used to define the mathematical model. The problem is solved using the analytical method given by Sankarsubramanian and Gill to find the temperature and velocity of nanofluid and the transport coefficients of nanobiosensors. MATLAB was used plot the graphs and see the variation of different parameters like slip parameter, stenosis depth and nanolayer thickness. It was found that once the nanobiosensors were dispersed, the temperature escalated as the nanobiosensors hit the stenosis. If the stenosis depths are around $0.1x10^{(-3)}$ m to $0.3x10^{(-3)}$ m, in a diseased artery, then nano-biosensors with a layer thickness of about 30 nm shall be suitable for the temperature range of 310-320K. This mathematical model bears possible applications in target detection and drug delivery at stenosed sites.

Keywords- Nanofluid, Nano biosensors, Dispersion, Stenosis.

1. Introduction

Cardiovascular diseases (CVDs) are the prime reason of mortality since many years. In 2021, almost 20.5 million people suffered from to cardiovascular disorders, reckoning at about one-third of deaths throughout the globe. There has been a substantial increase in 12.1 million CVD deaths since 1990. Although there have been major developments in medical research and treatment, there has been a decline in CVD related deaths, but still not sufficient to meet target laid by the World Health Assembly's (WHA) to reduce premature deaths occurring out of noncommunicable diseases (NCDs) to 25% by 2025 (World Heart Federation, 2023). Besides, the COVID-19 pandemic, to a great extent, disrupted world health concerns, straining healthcare systems and intensifying resource restraints. Thus, developing affordable, convenient, and efficient diagnostic tools capable of fast diagnostics and cure is a necessity (Malik et al., 2013).

Research designates that more than 80% of cardiovascular disease related deaths are associated with weakened blood flow, mostly due to diseases like atherosclerosis. Atherosclerosis is the buildup of fatty deposits in lining of arterial walls, ending up in plaque development that curbs blood flow and serious constitute health perils. Stenosis is a condition of narrowing of blood vessels triggered by plaque buildup, that intensifies these diseased conditions by further cutting back blood flow.

Improvements in diagnostic skills and technologies for atherosclerosis are vital for an early detection and treatment. Conventional approaches such as catheterization, while effective, are often sluggish and resource-concentrated. Thus, there is a pressing need to develop rapid, reliable, and cost-effective diagnostic tools that hold the capability of detecting atherosclerosis in its premature stage, significantly refining patient consequences (Sagadevan and Periasamy, 2014). Biosensors extend a potential resolution by coalescing nanomaterials into diagnostic tools, allowing for detailed and effectual detection of ailments.

Biosensors have myriad applications, extending from environmental pollution detection, food quality monitoring to disease diagnostics. These devices are sensitive to target compounds in samples that do not damage them and rather give continuous, reversible responses. A typical biosensor has a bioreceptor layer that detects molecular species such as antibodies, enzymes, or proteins and interprets these interactions into measurable signals applying various techniques, such as optical or electrochemical signals (Kiran and Mahesh, 2016).

The progress in biosensors has advanced over time. In 1956, American biochemist L. L. Clark invented the first biosensor to detect oxygen levels in blood (Arndt et al., 2020). Since then, biosensors have evolved through five generations. Earlier biosensors focused on detecting the analyte and bioreceptor reaction product to produce signals. For example, in the 1960s, Leland Charles Clark Jr. invented an enzyme electrode for glucose detection, and further advancements in the 1970s and 1980s caused the development of higher sensitive and more reliable biosensors. Today's biosensors unify nanotechnology for improved sensitivity, and cost-efficiency (Huang et al., 2021).

Nanotechnology has restructured biosensing by allowing for better accuracy along with nanoscale size. Nanobiosensors, employ nanoscale materials such as carbon nanotubes, graphene, and quantum dots to detect diseases early and precisely. These have several advantages, comprising boosted surface-to-volume ratios, greater electrical conductivity, and enhanced biocompatibility, making them ideal in diagnostic related applications (Naresh and Lee, 2021; Singh and Melnik, 2021).

A notable use of nanobiosensors holds in drug delivery systems. These sensors are target specific, as they detect stenosed arteries, and release drugs at the diseased location. Nanobiosensors make use of the properties of nanoparticles to increase drug transport, enhance circulation time, and advance targeting accuracy (Kulkarni et al., 2022).

The essential concept of a biosensor includes binding a bio analyte to bioreceptors, seizing the subsequent physiochemical change, and adapting it into a measurable signal through a transducer (Malik et al., 2023). This transducer is frequently attached with nanomaterials to generate nanobiosensors (Ramesh et al., 2023). These nanobiosensors in return have a specialized layer that detects the target analyte (Singh et al., 2023). Among the several nanomaterials, carbon nanotubes (CNTs) project as an important component for biosensor advancement in clinical diagnostics (Lee and Kim, 2024). When united with biological materials like enzymes or antibodies, CNTs indicatively boost precise responses.

CNTs are amongst the extensively utilized nanomaterials in biosensors, serving as frameworks to restrain biomolecules on their exterior (Tîlmaciu and Morris, 2015). Carbon nanotubes, primarily reported by Sumio Iijima in 1991 (Ferrier and Honeychurch, 2021; Gergeroglu et al., 2020), are categorized by their hollow, nanoscale construction comprising of carbon atoms. Their extraordinary durability, robustness, and capability to provide a platform for arresting biomolecules have made them focal to biosensor progress in both medical and research areas. CNTs are roughly 100,000 times compact than a human hair, which allows for an enormous possibility for transporting data from the nanoscale to the macroscopic extent. These extraordinary characteristics-along with their mechanical power and functionalization abilities-allow for the strategy of high-performance biosensors.

For drug delivery uses, nanobiosensors should be prompted by external stimuli, like alterations in temperature or pH or surface charge, or concentration, in order to release drugs at the desired target. Thermal nanobiosensors are triggered by temperature fluctuations, using the heat energy absorbed or released through biochemical reactions. These biosensors quantify the temperature change (ΔT), which is corelated

with the enthalpy (ΔH) of the reaction and the number of product molecules (np) produced, as signified by the equation $\Delta T = -(np\ \Delta H)/Cp$ (Lee and Kim, 2024). This classically includes a flow inoculation investigation with a restrained enzyme reactor, where the heat produced in a catalytic reaction is pondered by a thermally sensitive nanolayer. Such schemes have numerous advantages, comprising reduced sizes, low-cost manufacture, and great sensitivity, making them perfect for clinical uses (Lee and Kim, 2024).

Primary studies by Shah (2009) fixated on particle adhesion dynamics, predominantly in nanomedicine and biosensor applications. His mathematical simulation discovered the performance of micro/nano-scale particles dispersed in blood in stenotic arteries, placing the basis for forthcoming advances in biosensor technology and drug delivery systems. El Koumy et al. (2013) modelled peristaltic motion in a porous channel along with electrically conducting Maxwell fluid in a transverse magnetic field and Hall effect, examining parameters like porosity and permeability. Results provided understandings of flow dynamics, bearing possible applications in considering gall bladder function with stones. Recent research by Bali and Prasad (2022) based on the mathematical study of nanoparticle dispersion, precisely associating analytical and numerical solutions for nanoparticle performance in arteries with elliptical stenosis. This study emphasised the significance of correctly modelling several shapes and sizes of nanoparticles for an improved understanding of their circulation in stenotic arteries.

Muthtamilselvan and Gifteena Hingis (2022) contributed to this research by inspecting the flow features of nanoparticles in multi-stenosed arteries. Their work focused on the functioning of biosensors and the arterial walls, providing perceptions into how nanoparticles can circumnavigate multifaceted geometries to attain targeted drug delivery. Another noteworthy influence was made by Alhussain (2022), who modelled the thermal conductivity of nanoparticles in multi-stenosed arteries. This work established how thermal properties of nanoparticles effect their movement and adhesion inside the bloodstream, additionally improving our understanding of nanobiosensor conduct in real biological conditions.

Building upon these previous studies, Shamloo et al. (2023) established an in-silico model to simulate the transportation of nanocarriers in blood vessels, further enhancing the computational tools essential for reviewing nanoparticle dispersion in multi-stenosed arteries. Abdelsalam et al. (2023) explored the flow of a non-Newtonian Maxwell fluid over a permeable stretching sheet in a porous medium, integrating the Cattaneo-Christov heat flux model to investigate heat transfer in varying viscosity, magnetic fields, and thermal effects. Raju et al. (2024) deliberated the character of gold nanoparticles in stenosed arteries. Their study employed finite difference calculations to simulate the actions of these particles in dissimilar arterial situations, contributing appreciated understandings in the hemodynamics of nanoparticles in the treatment of stenosis. Similarly, Karmakar and Das (2024) examined magnetic nanoparticles and their dispersion in electroosmotic forces in a stenosed artery. Their study combined electro-magnetic forces and non-Newtonian blood flow properties, progressing our understanding of how nanoparticles perform in dynamic and complex vascular surroundings. Furthermore, Sayah et al. (2024) observed the drug delivery possibility of nanoparticles in stenotic arteries, accenting the size and shape of nanocarriers. Their work delivered serious visions into the ideal settings for drug delivery systems, directing on the adhesion of nanoparticles to atherosclerotic plaque in arteries. Abdelsalam et al. (2024b) studied peristaltic motion of hybrid nanofluids in a curved asymmetric channel with heated sinusoidal walls, arising exact solutions in long wavelength and low Reynolds number approximations. Abdelsalam et al. (2024a) inspected magnetohydrodynamic flow and thermal radiation effects on gold nanoparticle (AuNP) nanofluids in blood vessels, concentrating on nanoparticle shapes, peristalsis, and heat transfer properties. Adhikari et al. (2024) explored the combination of hybrid nanoparticles and microbes in an elastic artery with stenosis. Raza et al. (2024) studied the heat and mass transfer mechanisms in Carreau nano liquid flow over an extendable rotating disk, integrating effects of viscous dissipation, Joule heating, and nonlinear thermal radiation.

Kumar et al. (2024) observed electrokinetic peristaltic flow of Sutterby nanofluid in an asymmetric porous microchannel under transverse magnetic and longitudinal electric fields.

Upon this literature survey, this study is an attempt to fill a gap in present research by exploring the dispersion of nanobiosensors in arteries with multiple stenoses. While earlier research has explored nanobiosensor performance in single stenosis situations, there is inadequate data on how nanobiosensors perform in more complex arterial situations. By applying nonlinear Navier-Stokes equations and using carbon nanotubes as the nanobiosensors, this study examines their performance in response to thermal stimuli in a multi-stenosis artery model. The mathematical model is constructed on the equations of continuity, Navier-Stokes, and diffusion, and the dispersion of carbon nanotubes (Shobha and Muniraj, 2012) is solved applying the Subramanian and Gill (1973) model. Outcomes are presented graphically using MATLAB, delivering understandings that could direct upcoming clinical applications and treatment approaches.

The research article is hence an effort to a bridge the gap of theoretical modelling and practical biomedical applications. By delivering an inclusive mathematical outline, the study interprets complex fluid dynamics into actionable perceptions that can enhance biosensor strategy aimed at real-world situations, such as directing the asymmetrical flow in arteries with stenosis. This shall be helpful to engineers and medical professionals, to enhance nanobiosensors for applications like targeted drug delivery and diagnostic imaging, guaranteeing they perform proficiently under adjustable biological settings. The mathematical model offers analytical perceptions that decrease the necessity for extensive experimental trials, controlling the advancement of next-generation medical devices for real-time monitoring and nominally invasive treatments. Moreover, the research improves the accuracy and productivity of drug delivery systems by explicating how features like stenosis depth affect biosensor movement and dispersion, thus refining treatment results. It also delivers an outline for supervisory and clinical validation by contributing simulations that can be used to design further effective clinical trials. Additionally, this study enables cross-disciplinary collaboration between mathematicians, engineers, and medical professionals, helping to quicken the transformation of theoretical research into practical, patient-centred resolutions. Eventually, this work develops to the amalgamation of nanobiosensor-based technologies into clinical practice. It contributes to the increasing frame of knowledge on nanotechnology-enabled diagnostics and treatments. The conclusions regarding nanolayer on nanobiosensors provide valuable theoretical understandings and real-world consequences for evolving more effective diagnostic tools and drug delivery systems, possibly refining the management of cardiovascular diseases.

2. Mathematical Formulation

Mathematical modelling plays a pivotal role in elucidating the dispersion dynamics of nanobiosensors within arteries with multiple stenosis, offering valuable insights into their behaviour and potential applications in biomedical engineering and healthcare. The approach to develop mathematical model here includes the injection of thermal nanobiosensors into the artery which is then analysed under steady state conditions. The arterial geometry, blood flow characteristics and nanobiosensors' nature have been taken into consideration to from the model. An artery of length L' is considered with multiple stenosis (**Figure 1**). Cylindrical co-ordinates (r', θ', z') are taken into account. **Table 1** lists the mathematical symbols to be used.

The geometry of stenosis (Muthtamilselvan and Gifteena Hingis, 2022) is given as:

$$R'(z') = \begin{cases} R_0\left(1 - \frac{\delta'_i}{R_0 d'_i}\frac{i^{\frac{i}{i-1}}}{i-1}\left(s'_i(z'-d'_i) + (z'-d'_i)^i\right)\right), & d'_i \le z' \le d'_i + s'_i \\ R_o\ , & otherwise \end{cases} \quad (1)$$

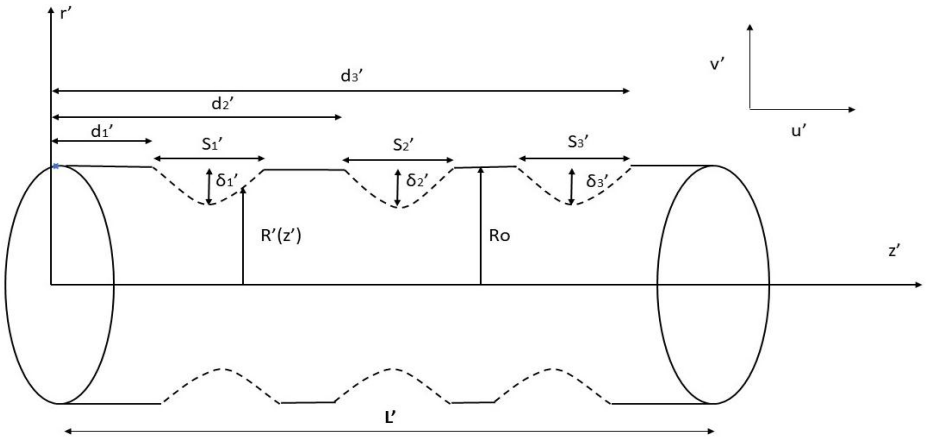

Figure 1. Geometrical model.

The equations modelling the blood flow with nanobiosensors are:

Equation of continuity

$$\frac{\partial \rho_{nf}}{\partial t'} + \frac{1}{r'}\frac{\partial (r\,\rho_{nf} u')}{\partial r'} + \frac{1}{r'}\frac{\partial \rho_{nf} v'}{\partial \theta'} + \frac{\partial \rho_{nf} w'}{\partial z'} = 0 \quad (2)$$

Navier Stokes momentum equation or equation of motion

$$\frac{\partial v'}{\partial t'} + v'\frac{\partial v'}{\partial r'} + \frac{u'}{r'}\frac{\partial v'}{\partial \theta'} - \frac{u'^2}{r'} + u'\frac{\partial v'}{\partial z'} = F_{r'} - \frac{1}{\rho_{nf}}\frac{\partial p'}{\partial r'} + \frac{\mu_{nf}}{\rho_{nf}}\left(-\frac{v'}{r^2} + \frac{1}{r'}\frac{\partial}{\partial r'}\left(r'\frac{\partial v'}{\partial r'}\right) + \right.$$

$$\left.\frac{1}{r'^2}\frac{\partial^2 v'}{\partial \theta'^2}\frac{\partial^2 v'}{\partial z'^2}\frac{2}{r'^2}\frac{\partial w'}{\partial \theta'}\right) \quad (3)$$

$$\frac{\partial w'}{\partial t'} + v'\frac{\partial w'}{\partial r'} + \frac{u'}{r'}\frac{\partial w'}{\partial \theta'} - \frac{v'w'}{r'} + u'\frac{\partial w'}{\partial z'} = F_{\theta'} - \frac{1}{\rho_{nf}}\frac{\partial p'}{\partial \theta'} + \frac{\mu_{nf}}{\rho_{nf}}\left(-\frac{w'}{r^2} + \frac{1}{r'}\frac{\partial}{\partial r'}\left(r'\frac{\partial w'}{\partial r'}\right) + \frac{1}{r'^2}\frac{\partial^2 w'}{\partial \theta'^2} + \right.$$

$$\left.\frac{\partial^2 w'}{\partial z'^2} + \frac{2}{r'^2}\frac{\partial v'}{\partial \theta'}\right) \quad (4)$$

$$\frac{\partial u'}{\partial t'} + v'\frac{\partial u'}{\partial r'} + \frac{u'}{r'}\frac{\partial u'}{\partial \theta'} + u'\frac{\partial u'}{\partial z'} = F_{z'} - \frac{1}{\rho_{nf}}\frac{\partial p'}{\partial z'} + \frac{1}{\rho_{nf}}\left(\frac{1}{r'}\frac{\partial}{\partial r'}\left(r'\frac{\partial u}{\partial r'}\right) + \frac{1}{r'^2}\frac{\partial^2 u'}{\partial \theta'^2} + \frac{\partial^2 u'}{\partial z'^2}\right) \quad (5)$$

Most current detection methods for low-concentration solutions are modelled by diffusion. The detection time *t'* is primarily determined by how long it takes for the target molecules to diffuse and interact with the probe molecules immobilized on the sensor surface, which are triggered thermally. The equations for this are:

Diffusion equation for temperature

$$\frac{1}{D_{nf}}\frac{\partial T\prime}{\partial t\prime}=\frac{\partial^2 T\prime}{\partial r\prime^2}+\frac{1}{r\prime}\frac{\partial T\prime}{\partial r\prime}+\frac{1}{r\prime^2}\frac{\partial^2 T\prime}{\partial \theta\prime^2}+\frac{\partial^2 T\prime}{\partial z\prime^2}+\frac{H}{k_{nf}} \tag{6}$$

Diffusion equation for concentration

$$\frac{1}{D\prime}\frac{\partial c\prime}{\partial t\prime}+u'\frac{\partial c'}{\partial z'}+\ v'\frac{\partial c'}{\partial r'}\ +w'\frac{\partial c\prime}{\partial \theta\prime}=\frac{\partial^2 c\prime}{\partial r\prime^2}+\frac{1}{r\prime}\frac{\partial c\prime}{\partial r\prime}+\frac{1}{r\prime^2}\frac{\partial^2 c\prime}{\partial \theta\prime^2}+\frac{\partial^2 c\prime}{\partial z\prime^2}+m' \tag{7}$$

where, D' signifies nanobiosensors' diffusivity while m' depicts the rate at which nanobiosensors are released in the blood or absorbed at the stenosis.

When nanoparticles are dispersed in a fluid, such as blood, the mixture is referred to as a nanofluid. Choi (Qiu et al., 2020) is accredited with the groundbreaking progress of nanofluids, which are colloidal systems of nanoparticles-such as metals, oxides, and carbon nanotubes-dispersed in a base fluid. These nanoparticles hold pointedly higher thermal conductivity than the base fluid unaided, and their size is characteristically less than *100 nm*. Nanofluids have quickly become a motivation of research due to their improved thermophysical properties, comprising amplified thermal conductivity and viscosity, making them chiefly appreciated for biomedical uses.

Thermal conductivity is a elementary thermophysical characteristic of nanofluid. Geomorphology, volume fraction, thermal conductivity of base fluid, thermal conductivity of nanoparticle dispersed are the features that regulate the thermal conductivity of a nanofluid. The first model was given by Maxwell in this regard. This was followed by series of experimental and theoretical researches. An advanced model for nanofluid's thermal conductivity was devised by Murshed et al. (2008) that inculcates the thermal conductivity of nanolayer also.

$$\frac{k_{nf}}{k_f}=\frac{\left(\frac{k_p}{k_f}-\frac{k_{nl}}{k_f}\right)\phi k_{nl}\left(2\left(1+\frac{dnl}{rp}\right)^3-\left(1+\frac{2dnl}{rp}\right)^3+1\right)+\left(\frac{k_p}{k_f}+2\frac{k_{nl}}{k_f}\right)\left(1+\frac{dnl}{rp}\right)^3\left(\phi\left(1+\frac{2dnl}{rp}\right)^3\left(\frac{k_{nl}}{k_f}-1\right)+1\right)}{\left[\left(1+\frac{dnl}{rp}\right)^3\left(\frac{k_p}{k_f}+2\frac{k_{nl}}{k_f}\right)-\left(\frac{k_p}{k_f}-\frac{k_{nl}}{k_f}\right)\phi\left(\left(1+\frac{dnl}{rp}\right)^3+\left(1+\frac{2dnl}{rp}\right)^3-1\right)\right]} \tag{8}$$

where, k_f is base fluid's thermal conductivity of base fluid, k_p is nanobiosensors' thermal conductivity, k_{nl} is nanolayer's thermal conductivity, dnl is thickness of nanolayer (on biosensor), r_p is radius of nanobiosensor and ϕ represents nanobiosensors' volume fraction. This empirical model is apt for nano biosensors as they, have a sensor coating of nanolayer on them to identify and transfer signals. Another important property in the hierarchy is viscosity of nanofluids. The prime model was formulated by Einstein. Batchelor (1977) proposed a model for viscosity of nanofluids by taking into account the Brownian motion of nanoparticles.

$$\mu_{nf}=\mu_f(1+A_1\phi+A_2\phi^2) \tag{9}$$

The factor A_1 represents the coefficient from Einstein's dynamic viscosity model and A_2 represents Huggin's coefficient that describes the viscosity due to thermal motion of nanoparticle. The value of A_1 is *13.5* and A_2 is *904.4* for carbon nanotubes.

The model for thermal expansion of nanofluid is written using rule of conservation of mass of two materials or species.

$$\rho\gamma_{nf}=(1-\phi)\rho\gamma_f+\phi\rho\gamma_p \tag{10}$$

The governing Equations (2) to (7) shall assumes:

i. Flow is steady, laminar and incompressible.
ii. Flow is axisymmetric.
iii. Azimuthal component is zero, thus, the flow is two dimensional.
iv. The cross-section area is narrow thus describing the flow by low Reynolds number.
v. The dispersion of nano biosensors takes place in response to temperature stimulus governed by the factor H, called the heat source parameter.
vi. Free convection effects are not considered.

Equations together with their boundary conditions are.

Equation of continuity

$$\frac{\partial \rho_{nf} u\prime}{\partial z\prime} = 0 \tag{11}$$

Navier Stokes equation accompanied with its boundary conditions

$$-\frac{\partial P'}{\partial z'} - \frac{1}{r'}\frac{\partial}{\partial r'}\left(r'\mu_{nf}\frac{\partial u\prime}{\partial r\prime}\right) + g(\rho\gamma)_{nf}(T' - T_0) = 0 \tag{12}$$

Since the flow is axis symmetric

$$\frac{\partial u\prime}{\partial r\prime} = 0 \text{ at } r' = 0 \tag{13}$$

Applying Darcy's law at arterial boundary of the artery because the nanobiosensors are absorbed at the stenosis

$$u' = u'_B \text{ at } r' = R_0 \tag{14}$$

$$\frac{\partial u\prime}{\partial r\prime} = \frac{\sigma'}{\sqrt{k'_0}}(u'_B - u'_p) \text{ at } r' = R_0 \tag{15}$$

where,

$$u'_p = -\frac{k\prime_0}{\mu_{nf}}\frac{\partial p\prime}{\partial z\prime} \tag{16}$$

is velocity at arterial boundary which is permeable.

where, u'_B represents velocity of slip, σ' is parameter of slip, k'_0 represents permeability of arterial wall.

Diffusion equation for temperature and its boundary conditions

$$\frac{\partial^2 T\prime}{\partial r\prime^2} + \frac{1}{r\prime}\frac{\partial T\prime}{\partial r\prime} + \frac{H}{k_{nf}} = 0 \tag{17}$$

Temperature is T_0 on surface of artery

$$T' = T_0 \text{ at } r' = R'(z') \tag{18}$$

By axis symmetricity

$$\frac{\partial T\prime}{\partial r\prime} = 0 \; at \; r' = 0 \tag{19}$$

Diffusion equation for concentration

$$\frac{\partial c\prime}{\partial t\prime} + u'\frac{\partial c\prime}{\partial z\prime} = D_m\left(\frac{1}{r'}\frac{\partial}{\partial r'}\left(r'\frac{\partial c'}{\partial r'}\right) + \frac{\partial^2 c'}{\partial z'^2}\right) \tag{20}$$

The nano biosensors are distributed uniformly therefore their concentration initially is

$$c'(0,z',r') = \omega'(z')\xi'(r') = c_o' \tag{21}$$

where,

$$\omega'(z') = \frac{R_0\delta(z')}{d'^2} \tag{22}$$

$\delta(z')$ is the Dirac Delta function

and

$$\xi'(r') = \begin{cases} 1 & 0 < r' \le d' \\ 0 & d' < r' \le R_0 \end{cases} \tag{23}$$

where, d' is initial distribution or placing of nanobiosensors.

At the onset

$$c'(t',z',r') = finite\ at\ r' = 0 \tag{24}$$

Diffusion of nano biosensors at artery's wall (Shobha and Muniraj, 2012) is

$$\frac{\partial c'(t',z',r')}{\partial t'} = k_0'\big(c'(0,z',r') - c'(t',z',r')\big)\rho_{nf} \text{ at } r' = R_0 \tag{25}$$

where, $k_0{}'$ is the conductivity of nano biosensors that are conjugated at the stenosis.

Since there are finite number of nano biosensors, hence at any random time

$$c'(t'z',r') = \frac{\partial c\prime(t',z',r')}{\partial z\prime} = 0 \text{ at } z' = \infty \tag{26}$$

Scheme for nondimensionalization

$$r = \frac{r\prime}{R_0},\ z = \frac{z\prime}{R_0},\ \theta = \frac{T\prime}{T_0},\ Gr = \frac{g\gamma_f\rho_f R_0^2 T_o}{u_{avg}\mu_f},\ h = \frac{HR_0^2}{T_0 k_f},\ Re = \frac{R_0 u_{avg}\rho_f}{\mu_f},\ Da = \frac{k\prime_o}{R_0^2},\ u = \frac{u\prime}{u_{avg}},\ p = \frac{R_0 p\prime}{\mu_f u_{avg}},\ \sigma = \frac{\sigma\prime}{R_0},\ t = \frac{D_m t\prime}{R_0^2},\ Pe = \frac{R_0 u_{avg}}{D_m},\ c = \frac{c\prime}{c_\alpha},\ \beta = \frac{k\prime_0 R_0}{D_m} \tag{27}$$

where, Da represents Darcy number, Gr represents Grashof number, Re is Reynolds number, Pe is Peclet number, u_{avg} is reference velocity, c_α is reference concentration and β is non-dimensional wall absorption parameter.

The nondimensional equations and boundary conditions are:

$$-Re\frac{\partial p}{\partial z} = \frac{1}{r}\frac{\partial}{\partial r}\left(r\mu_f(1 + A_1\phi + A_2\phi^2)\frac{\partial u}{\partial r}\right) + \left((1-\phi) + \frac{\phi\rho_p\gamma_p}{\rho_f\gamma_f}\right)Gr\theta \tag{28}$$

$$\frac{\partial^2\theta}{\partial r^2} + \frac{1}{r}\frac{\partial\theta}{\partial r} + h\frac{\left(\frac{k_p}{k_f}-\frac{k_{nl}}{k_f}\right)\phi k_{nl}\left(2\left(1+\frac{dnl}{r_p}\right)^3 - \left(1+\frac{2dnl}{r_p}\right)^3 + 1\right) + \left(\frac{k_p}{k_f}+2\frac{k_{nl}}{k_f}\right)\left(1+\frac{dnl}{r_p}\right)^3 (\phi\left(1+\frac{2dnl}{r_p}\right)^3\left(\frac{k_{nl}}{k_f}-1\right)+1)}{[\left(1+\frac{dnl}{r_p}\right)^3\left(\frac{k_p}{k_f}+2\frac{k_{nl}}{k_f}\right) - (\frac{k_p}{k_f}-\frac{k_{nl}}{k_f})\phi(\left(1+\frac{dnl}{r_p}\right)^3 + \left(1+\frac{2dnl}{r_p}\right)^3 - 1)]} = 0 \tag{29}$$

$$\frac{\partial c}{\partial t} + u\frac{\partial c}{\partial z} = \frac{1}{r}\frac{\partial}{\partial r}\left(r\frac{\partial c}{\partial r}\right) + \frac{1}{Pe^2}\frac{\partial^2 c}{\partial z^2} \tag{30}$$

$$\frac{\partial u}{\partial r} = 0 \text{ at } r = 0 \tag{31}$$

$$u = u_B \text{ at } r = 1 \tag{32}$$

$$\frac{\partial u}{\partial r} = \frac{\sigma}{\sqrt{Da}}(u_B - u_p) \text{ at } r = 1 \tag{33}$$

Here

$$u_p = -\frac{Da}{\mu_f(1+A_1\phi+A_2\phi^2)}\frac{\partial p}{\partial z} \text{ at } r = 1 \tag{34}$$

$$\theta = 1 \text{ at } r = 1 \tag{35}$$

$$\frac{\partial \theta}{\partial r} = 0 \text{ at } r = 0 \tag{36}$$

$$c_0 = \omega(z)\xi(r) \text{ where } \omega(z) = \frac{\delta(z)}{d^2 Pe} = c_0 \tag{37}$$

$$\xi(r) = \begin{cases} 1 & 0 < r \le d \\ 0 & d \le r \le 1 \end{cases}$$

$$c = finite \; at \; r = 0 \tag{38}$$

$$\frac{\partial c}{\partial t} = \beta(c_o - c) \; at \; r = 1 \tag{39}$$

$$c = \frac{\partial c}{\partial z} = 0 \text{ at } z = \infty \tag{40}$$

3. Solution

The Equation (29) has been solved analytically using the boundary conditions (35) and (36), and the value of θ or temperature of blood with nanobiosensors in it is obtained as:

$$\theta = 1 + h\frac{(R^2(z)-r^2)}{4}\frac{\left(\frac{k_p}{k_f}-\frac{k_{nl}}{k_f}\right)\phi k_{nl}\left(2\left(1+\frac{dnl}{r_p}\right)^3-\left(1+\frac{2dnl}{r_p}\right)^3+1\right)+\left(\frac{k_p}{k_f}+2\frac{k_{nl}}{k_f}\right)\left(1+\frac{dnl}{r_p}\right)^3\left(\phi\left(1+\frac{2dnl}{r_p}\right)^3\left(\frac{k_{nl}}{k_f}-1\right)+1\right)}{\left[\left(1+\frac{dnl}{r_p}\right)^3\left(\frac{k_p}{k_f}+2\frac{k_{nl}}{k_f}\right)-\left(\frac{k_p}{k_f}-\frac{k_{nl}}{k_f}\right)\phi\left(\left(1+\frac{dnl}{r_p}\right)^3+\left(1+\frac{2dnl}{r_p}\right)^3-1\right)\right]} \tag{41}$$

Using this value in Equation (28), and applying the boundary conditions (31) to (34), the velocity is found to be:

$$u = -Re\frac{\partial p}{\partial z}\frac{r^2}{4\mu_f(1+A_1\phi+A_2\phi^2)} - \frac{\left(\left((1-\phi)+\frac{\phi\rho_p\gamma_p}{\rho_f\gamma_f}\right)Gr\right)}{\mu_f(1+A_1\phi+A_2\phi^2)}\left(\frac{r^2}{4}+\left(\frac{r^2}{4}R^2(z) - \right.\right.$$

$$\left.\left.\frac{r^4}{16}\right)\frac{\left(\frac{k_p}{k_f}-\frac{k_{nl}}{k_f}\right)\phi k_{nl}\left(2\left(1+\frac{dnl}{r_p}\right)^3-\left(1+\frac{2dnl}{r_p}\right)^3+1\right)+\left(\frac{k_p}{k_f}+2\frac{k_{nl}}{k_f}\right)\left(1+\frac{dnl}{r_p}\right)^3\left(\phi\left(1+\frac{2dnl}{r_p}\right)^3\left(\frac{k_{nl}}{k_f}-1\right)+1\right)}{\left[\left(1+\frac{dnl}{r_p}\right)^3\left(\frac{k_p}{k_f}+2\frac{k_{nl}}{k_f}\right)-\left(\frac{k_p}{k_f}-\frac{k_{nl}}{k_f}\right)\phi\left(\left(1+\frac{dnl}{r_p}\right)^3+\left(1+\frac{2dnl}{r_p}\right)^3-1\right)\right]}\right) + \mu_f(1+A_1\phi+A_2\phi^2)u_p - \left(\frac{1}{4}-\right.$$

$$\left.\frac{\sqrt{Da}}{2\sigma}\right)\left(-Re\frac{\partial p}{\partial z}+\left(\left((1-\phi)+\frac{\phi\rho_p\gamma_p}{\rho_f\gamma_f}\right)Gr\right)+\left(\left((1-\phi)+\right.\right.\right.$$

$$\left.\left.\left.\frac{\phi\rho_p\gamma_p}{\rho_f\gamma_f}\right)Gr\right)\frac{\left(\frac{k_p}{k_f}-\frac{k_{nl}}{k_f}\right)\phi k_{nl}\left(2\left(1+\frac{dnl}{r_p}\right)^3-\left(1+\frac{2dnl}{r_p}\right)^3+1\right)+\left(\frac{k_p}{k_f}+2\frac{k_{nl}}{k_f}\right)\left(1+\frac{dnl}{r_p}\right)^3\left(\phi\left(1+\frac{2dnl}{r_p}\right)^3\left(\frac{k_{nl}}{k_f}-1\right)+1\right)}{\left[\left(1+\frac{dnl}{r_p}\right)^3\left(\frac{k_p}{k_f}+2\frac{k_{nl}}{k_f}\right)-\left(\frac{k_p}{k_f}-\frac{k_{nl}}{k_f}\right)\phi\left(\left(1+\frac{dnl}{r_p}\right)^3+\left(1+\frac{2dnl}{r_p}\right)^3-1\right)\right]}\left(R^2(z)-\frac{1}{2}\right)\right) \tag{42}$$

The process of nanoparticle deposition at a target site involves three stages. First, nanoparticles must marginate from the bloodstream toward the vascular wall, via convection. The dispersion of nanobiosensors in the artery can be described by the convection and diffusion process, and finally when the nanobiosensors hit the stenosis, it is governed by diffusion at the permeable walls observed particularly at the nanoscale. Now, in order to solve the equation for dispersion, the method employed by Sankarasubramanian and Gill (1973) is used, which will result in three transport coefficients explaining this phenomenon.

A series solution is assumed for c as

$$c = \sum_{i=0}^{\infty} \psi_i \frac{\partial c_m}{\partial z^i} \tag{43}$$

where, mean concentration of nanobiosensors c_m is

$$c_m = 2\int_0^1 cr\, dr \text{ and } \psi_i(t,r), i = 0,1,2, \text{ has time and radial distance as parameters} \tag{44}$$

Equation (30) after being multiplied with $2r$ and integrated for r for limits 0 to 1

$$\frac{\partial c_m}{\partial t} = \frac{1}{Pe^2}\frac{\partial^2 c_m}{\partial z^2} + 2\frac{\partial c}{\partial r}\Big|_{r=1} - 2\frac{\partial}{\partial z}\int_0^1 ucr\, dr \tag{45}$$

The dispersion equation in c_m along with time dependable transport coefficient by using Equation (43) in Equation (45)

$$\frac{\partial c_m}{\partial t} = \sum_{i=0}^{\infty} K_i \frac{\partial^i c_m}{\partial z^i} \tag{46}$$

Here

$$K_i = \frac{\delta_{i2}}{Pe^2} + 2\frac{\partial \psi_i}{\partial r}\Big|_{r=1} - 2\int_0^1 \psi_{i-1}\, ur\, dr,\ i = 0,1,2,\ldots\ldots,\ \psi_{-1} = 0 \tag{47}$$

$$\text{Here } \delta_{ij} = \begin{cases} 1 & i = j \\ 0 & i \neq j \end{cases} \tag{48}$$

The final dispersion model is

$$\frac{\partial c_m}{\partial t} = K_0 c_m + K_1 \frac{\partial c_m}{\partial z} + K_2 \frac{\partial^2 c_m}{\partial z^2} \tag{49}$$

Here,

$$K_i = \frac{\delta_{i2}}{Pe^2} + 2\frac{\partial \psi_i}{\partial r}\Big|_{r=1} - 2\int_0^1 \psi_{i-1}\, ur\, dr,\ i = 0,1,2 \tag{50}$$

The transport coefficient K_0 indicates the presence of nanobiosensors at the artery wall where they hit the stenosed site, K_1 arises out of the convections of nano biosensor and K_2 signifies dispersion coefficient which is the combined effect of diffusion and nanobiosensors' velocity in blood. K_i for $i = 3,4,5.$ provide no significant contribution as dispersion reaches the steady state.

The nanobiosensors' concentration is

$$c = \sum_{i=0}^{2} \psi_i \frac{\partial^i c_m}{\partial z^i} \tag{51}$$

For solving Equations (48) and (49), the boundary conditions need to be found. Using Equation (49) in Equation (30). Equating coefficients of $\frac{\partial^l c_m}{\partial z^l}$ for $l = 0,1,2$ and obtaining

$$\frac{\partial \psi_i}{\partial t} = \frac{1}{r}\frac{\partial}{\partial r}\left(r\frac{\partial \psi_i}{\partial r}\right) - u\psi_{l-1} + \frac{1}{Pe^2}\psi_{l-2} - \sum_{i=0}^{l} K_i \psi_{l-i}$$

where, $l = 0, 1, 2$ (52)

and
$\psi_{-1} = \psi_{-2} = 0$ (53)

Conditions designated with the help of Equations (37) to (40), as
$c_m = 2\omega \int_0^1 \xi r \, dr$ at $t = 0$ (54)

$\psi_0 = \frac{\xi}{2\int_0^1 \xi r \, dr}$ at $t = 0$ (55)

$\psi_l = 0, l = 1,2$ at $t = 0$ (56)

$\frac{\partial \psi_l}{\partial r} = 0, l = 0,1,2$ at $r = 0$ (57)

$\frac{\partial \psi_l}{\partial t} = \beta(\psi_0 - \psi_l), l = 1,2$ at $r = 1$ (58)

$c_m = \frac{\partial c_m}{\partial z} = 0$ at $z = \infty$ (59)

Using Equation (52) in Equation (49), one more condition is obtained
$\int_0^1 \psi_l \, r \, dr = \frac{1}{2}\delta_{l0}$ for $l = 0,1,2$ (60)

where, δ_{l0} is defined by Equation (47)

The value of ψ_0 and K_0 are not dependent of nanofluid velocity, hence are obtained directly applying the boundary conditions (52)
$\frac{\partial \psi_0}{\partial t} = \frac{1}{r}\frac{\partial}{\partial r}\left(r\frac{\partial \psi_0}{\partial r}\right) - K_0\psi_0$ (61)

With an additional condition on ψ_0 as $\int_0^1 \psi_0 \, r \, dr = 1/2$ (62)

Solution to non- homogeneous boundary value problem (61) employing Bessel equation fulfilling conditions (54) - (59) along with Equation (62) is found now.
Let $\psi_0(t,r) = e^{\{-\int_0^t K_0(\eta)d\eta\}}\varrho(t,r)$ (63)

Using this transformation (63), equation of $\varrho(t,r)$ is found that should fulfil
$\frac{\partial \varrho}{\partial t} = \frac{1}{r}\frac{\partial}{\partial r}r\frac{\partial \varrho}{\partial r}$ (64)

$\varrho(0,r) = \psi_0(0,r) = \frac{\xi(r)}{2\int_0^1 r\xi(r)dr}$ (65)

$\frac{\partial \varrho}{\partial r}(t,1) = \beta(\varrho(0,1) - \varrho(t,1))$ (66)

$\varrho(t,0) = finite$ (67)

Assume solution to be as
$\varrho(t,r) = \sum_{m=0}^{\infty} A_m e^{-\lambda_m^2 t}$ (68)

Using (Philip, 1957) identity

$$(\frac{\partial \varrho}{\partial t})_r(\frac{\partial r}{\partial \varrho})_t = -(\frac{\partial r}{\partial t})_\varrho \tag{69}$$

Converting Equation (64) as

$$-\frac{1}{2}\frac{\partial r^2}{\partial t} = \frac{\partial}{\partial \varrho}(r\frac{\partial \varrho}{\partial r}) \tag{70}$$

Integrating with respect to ϱ gives

$$-\frac{1}{2}\frac{\partial}{\partial t}\int_{\varrho_0}^{\varrho} r^2 d\varrho = \left(r\frac{\partial \varrho}{\partial r}\right) \tag{71}$$

Substituting Equation (68) into Equation (71), solution to $\varrho(t,r)$ is found after equating coefficients of either side, solution of Equations (64) to (67) is

$$\varrho(t,r) = \sum_{m=0}^{\infty} A_m J_0(\lambda_m r) e^{-\lambda_m^2 t} \tag{72}$$

Now, using Equation (68), we get

$$\psi_0 = \frac{\sum_{m=0}^{\infty} A_m J_0(\lambda_m r) e^{-\lambda_m^2 t}}{2\sum_{m=0}^{\infty}(\frac{A_m}{\lambda_m}) J_1(\lambda_m) e^{-\lambda_m^2 t}} \text{ where, } J_0 \text{ and } J_1 \text{ represent Bessel functions} \tag{73}$$

and λ_m are roots of equation given below

$$e^{-\lambda_m^2 t}(\beta - \lambda_m^2) = \beta J_0(\lambda_m),\ m = 0, 1, 2, \ldots \tag{74}$$

Also,

$$A_m = \frac{2}{[J_1(\lambda_m)]^2}\int_0^1 r \sum_{m=0}^{\infty} A_m J_o(\lambda_m r) J_o(\lambda_m r) dr,$$
$$m = 0, 1, 2, \ldots \tag{75}$$

K_0 is found as

$$K_0 = 2\frac{\partial \psi_0}{\partial r}\Big|_{r=1} = -\frac{\sum_{m=0}^{\infty} A_m \lambda_m J_1(\lambda_m) e^{-\lambda_m^2 t}}{\sum_{m=0}^{\infty}\left(\frac{A_m}{\lambda_m}\right) J_1(\lambda_m) e^{-\lambda_m^2 t}} \tag{76}$$

In case of steady state, $t \to \infty$, thus, Equations (50) and (66) give the value of function ψ_0 and K_0 as

$$\lim_{t\to\infty} \psi_0 = \frac{\lambda_0}{2J_1(\lambda_0)} J_0(\lambda_0 r) \text{ and } \lim_{t\to\infty} K_0 = -\lambda_0^2 \tag{77}$$

where, λ_0 is smallest root of Equation (74)

Since it is a steady flow, value of K_i, i=1, 2 is found from value of nanofluid velocity in Equation (42). ψ_i, i=1,2 in steady state condition is

$$\frac{1}{r}\frac{\partial}{\partial r}\left(r\frac{\partial \psi_l}{\partial r}\right) + \lambda_0^2 \psi_l = u\psi_{l-1} - \frac{1}{Pe^2}\psi_{l-2} + \sum_{i=1}^{l} K_i \psi_{l-i} + K_l \psi_0 \text{ where, } l\text{=1,2} \tag{78}$$

and

$$\psi_{-1} = 0 \tag{79}$$

K_i, i=1,2 reduce to under steady state

$$K_l = \frac{\delta_{l2}}{Pe^2} + 2\frac{\partial \psi_i}{\partial r}\Big|_{r=1} - 2\int_0^1 ru\psi_{l-1}\, dr\,, l = 1,2 \tag{80}$$

Conditions for $\psi_l,\ l = 1,2$

$$\psi_l = finite \text{ or } \frac{\partial \psi_l}{\partial r} = 0 \text{ at } r = 0,\ l = 1,2 \tag{81}$$

$$\frac{\partial \psi_l}{\partial t} = \beta(\psi_0 - \psi_l) \text{ at } r = 1\ ,\ l = 1,2 \tag{82}$$

$$\int_0^1 \psi_l r\, dr = 0, l = 1,2 \tag{83}$$

Equation (79) is the Strum-Liouville boundary value problem, solution for which is obtained applying orthogonality of eigen functions. The eigen function shall be orthogonal to Equation (80) with weight function *r.* So, solution to Equation (80) i.e.

$$\frac{1}{r}\frac{\partial}{\partial r}\left(r\frac{\partial \psi_l}{\partial r}\right) + \lambda_0^2 \psi_l = 0 \tag{84}$$

ψ_l is calculated by Bessel's function of zeroth order as $\psi_l = J_0(\lambda_0 r)$. Let it be represented eigen function

$$\phi_n = J_0(\lambda_0 r) \tag{85}$$

Multiplying both sides of Equation (80) by $r\phi_n$, left- side of Equation (80) nullifies and by the trait of orthogonal functions, K_l is found. Value of exchange coefficients $K_l, l = 1,2$ is in terms of $\psi_l, l = 1,2$

$$K_l = \frac{\int_0^1 r J_0(\lambda_0 r)(u\psi_{l-1} - \frac{1}{Pe^2}\psi_{l-2} + \sum_{i=1}^{l} K_i \psi_{l-i})dr}{\int_0^1 \psi_0 r J_0(\lambda_0 r) dr},\ l = 1,2 \tag{86}$$

The value of K_1

$$K_1 = \frac{\int_0^1 r J_0(\lambda_0 r) u\psi_0 dr}{\int_0^1 \psi_0 r J_0(\lambda_0 r) dr} = -\frac{2\lambda_0^2}{(\lambda_0^2 + \beta^2) J_0^2(\lambda_0)} \int_0^1 u r J_0^2(\lambda_0 r) dr \tag{87}$$

The value of ψ_1

$$\frac{1}{r}\frac{\partial}{\partial r}\left(r\frac{\partial \psi_1}{\partial r}\right) + \lambda_0^2 \psi_1 = u\psi_0 + K_1 \psi_0 \tag{88}$$

The boundary condition for ψ_1

$$\psi_1 = finite \text{ at } r = 0 \tag{89}$$

$$\frac{\partial \psi_1}{\partial t} = \beta(\psi_0 - \psi_1) \text{ at } r = 1 \tag{90}$$

$$\int_0^1 \psi_1 r\, dr = 0 \tag{91}$$

Putting K_l in Equation (86), we get ψ_1 fulfilling Equations (90) to (92) as

$$\psi_1 = \sum_{m=0}^{\infty} B_m J_0(\lambda_m r) \tag{92}$$

where, expansion coefficient B_0 by using Equations (91) and (92) is found in terms of B_j (j=1,2,…) as

$$B_0 = -\frac{\lambda_0}{J_1(\lambda_0)} \sum_{n=1}^{\infty} B_m \frac{J_1(\lambda_m)}{\lambda_m} \tag{93}$$

Using Equation (93) in Equation (92)

$$\psi_1 = \sum_{m=0}^{\infty} B_m \left(J_0(\lambda_m r) - \frac{\lambda_0}{J_1(\lambda_0)} \frac{J_1(\lambda_m)}{\lambda_m} J_0(\lambda_0 r)\right) \tag{94}$$

where,

$$B_m = \frac{2\lambda_m^2}{(\lambda_0^2-\lambda_m^2)(\lambda_m^2+\beta^2)J_0^2(\lambda_m)} \int_0^1 (u+K_1)\psi_0 r J_0(\lambda_m r)dr \tag{95}$$

The dispersion coefficient K_2 using Equations (87), (94) and (95) is

$$K_2 = \frac{1}{Pe^2} - \frac{4\lambda_0 J_1(\lambda_0)}{(\lambda_m^2+\beta^2)J_0^2(\lambda_m)} \int_0^1 (u+K_1)(\psi-\psi_1) r J_0(\lambda_0 r)dr \tag{96}$$

Thus,

$$K_1 = -2\int_0^1 r\, u\, dr \tag{97}$$

$$K_1 = -Re\frac{\partial p}{\partial z}\frac{1}{8\mu_f(1+A_1\phi+A_2\phi^2)} + \frac{\left(\left((1-\phi)+\frac{\phi\rho_p\gamma_p}{\rho_f\gamma_f}\right)Gr\right)}{\mu_f(1+A_1\phi+A_2\phi^2)}\left[\frac{1}{12} + \frac{\left(\frac{k_p}{k_f}-\frac{k_{nl}}{k_f}\right)\phi k_{nl}\left(2\left(1+\frac{dnl}{r_p}\right)^3-\left(1+\frac{2dnl}{r_p}\right)^3+1\right)+\left(\frac{k_p}{k_f}+2\frac{k_{nl}}{k_f}\right)\left(1+\frac{dnl}{r_p}\right)^3\left(\phi\left(1+\frac{2dnl}{r_p}\right)^3\left(\frac{k_{nl}}{k_f}-1\right)+1\right)}{\left[\left(1+\frac{dnl}{r_p}\right)^3\left(\frac{k_p}{k_f}+2\frac{k_{nl}}{k_f}\right)-\left(\frac{k_p}{k_f}-\frac{k_{nl}}{k_f}\right)\phi\left(\left(1+\frac{dnl}{r_p}\right)^3+\left(1+\frac{2dnl}{r_p}\right)^3-1\right)\right]}\frac{R^2(z)}{8} - \frac{\left(\frac{k_p}{k_f}-\frac{k_{nl}}{k_f}\right)\phi k_{nl}\left(2\left(1+\frac{dnl}{r_p}\right)^3-\left(1+\frac{2dnl}{r_p}\right)^3+1\right)+\left(\frac{k_p}{k_f}+2\frac{k_{nl}}{k_f}\right)\left(1+\frac{dnl}{r_p}\right)^3\left(\phi\left(1+\frac{2dnl}{r_p}\right)^3\left(\frac{k_{nl}}{k_f}-1\right)+1\right)}{\left[\left(1+\frac{dnl}{r_p}\right)^3\left(\frac{k_p}{k_f}+2\frac{k_{nl}}{k_f}\right)-\left(\frac{k_p}{k_f}-\frac{k_{nl}}{k_f}\right)\phi\left(\left(1+\frac{dnl}{r_p}\right)^3+\left(1+\frac{2dnl}{r_p}\right)^3-1\right)\right]}{32}\right] - \left[\mu_f(1+A_1\phi+A_2\phi^2)u_p - \left(\frac{1}{4}-\frac{\sqrt{Da}}{2\sigma}\right)\left(-Re\frac{\partial p}{\partial z} + \left(\left((1-\phi)+\frac{\phi\rho_p\gamma_p}{\rho_f\gamma_f}\right)Gr\right) + \left(\left((1-\phi)+\frac{\phi\rho_p\gamma_p}{\rho_f\gamma_f}\right)Gr\right)\frac{\left(\frac{k_p}{k_f}-\frac{k_{nl}}{k_f}\right)\phi k_{nl}\left(2\left(1+\frac{dnl}{r_p}\right)^3-\left(1+\frac{2dnl}{r_p}\right)^3+1\right)+\left(\frac{k_p}{k_f}+2\frac{k_{nl}}{k_f}\right)\left(1+\frac{dnl}{r_p}\right)^3\left(\phi\left(1+\frac{2dnl}{r_p}\right)^3\left(\frac{k_{nl}}{k_f}-1\right)+1\right)}{\left[\left(1+\frac{dnl}{r_p}\right)^3\left(\frac{k_p}{k_f}+2\frac{k_{nl}}{k_f}\right)-\left(\frac{k_p}{k_f}-\frac{k_{nl}}{k_f}\right)\phi\left(\left(1+\frac{dnl}{r_p}\right)^3+\left(1+\frac{2dnl}{r_p}\right)^3-1\right)\right]}\left(R^2(z)-\frac{1}{2}\right)\right)\right] \tag{98}$$

Now,

$$K_2 = \frac{1}{Pe^2} - 2\int_0^1 r\, u(\psi - \psi_1)dr \tag{99}$$

$$K_2 = \frac{1}{Pe^2} - 2\left(\psi - \sum_{l=1}^{\infty} B_l \frac{2\lambda_0 J_1(\lambda_l)}{J_1(\lambda_0)(\lambda_l)}\right)\left[-Re\frac{\partial p}{\partial z}\frac{1}{8\mu_f(1+A_1\phi+A_2\phi^2)} + \frac{\left(\left((1-\phi)+\frac{\phi\rho_p\gamma_p}{\rho_f\gamma_f}\right)Gr\right)}{\mu_f(1+A_1\phi+A_2\phi^2)}\left[\frac{1}{12} + \frac{\left(\frac{k_p}{k_f}-\frac{k_{nl}}{k_f}\right)\phi k_{nl}\left(2\left(1+\frac{dnl}{r_p}\right)^3-\left(1+\frac{2dnl}{r_p}\right)^3+1\right)+\left(\frac{k_p}{k_f}+2\frac{k_{nl}}{k_f}\right)\left(1+\frac{dnl}{r_p}\right)^3\left(\phi\left(1+\frac{2dnl}{r_p}\right)^3\left(\frac{k_{nl}}{k_f}-1\right)+1\right)}{\left[\left(1+\frac{dnl}{r_p}\right)^3\left(\frac{k_p}{k_f}+2\frac{k_{nl}}{k_f}\right)-\left(\frac{k_p}{k_f}-\frac{k_{nl}}{k_f}\right)\phi\left(\left(1+\frac{dnl}{r_p}\right)^3+\left(1+\frac{2dnl}{r_p}\right)^3-1\right)\right]}\frac{R^2(z)}{8} -$$

$$\frac{\left(\frac{k_p}{k_f}-\frac{k_{nl}}{k_f}\right)\phi k_{nl}\left(2\left(1+\frac{dnl}{r_p}\right)^3-\left(1+\frac{2dnl}{r_p}\right)^3+1\right)+\left(\frac{k_p}{k_f}+2\frac{k_{nl}}{k_f}\right)\left(1+\frac{dnl}{r_p}\right)^3\left(\phi\left(1+\frac{2dnl}{r_p}\right)^3\left(\frac{k_{nl}}{k_f}-1\right)+1\right)}{\left[\left(1+\frac{dnl}{r_p}\right)^3\left(\frac{k_p}{k_f}+2\frac{k_{nl}}{k_f}\right)-\left(\frac{k_p}{k_f}-\frac{k_{nl}}{k_f}\right)\phi\left(\left(1+\frac{dnl}{r_p}\right)^3+\left(1+\frac{2dnl}{r_p}\right)^3-1\right)\right]}}{32}\Bigg]-\Bigg(\psi-\sum_{l=1}^{\infty}B_l\frac{2\lambda_0 J_1(\lambda_l)}{J_1(\lambda_0)(\lambda_l)}\Bigg)\Bigg[\mu_f(1+A_1\phi+$$

$$A_2\phi^2)u_p-\left(\frac{1}{4}-\frac{\sqrt{Da}}{2\sigma}\right)\Bigg(-Re\frac{\partial p}{\partial z}+\left(\left((1-\phi)+\frac{\phi\rho_p\gamma_p}{\rho_f\gamma_f}\right)Gr\right)+\left(\left((1-\phi)+$$

$$\frac{\phi\rho_p\gamma_p}{\rho_f\gamma_f}\right)Gr\Bigg)\frac{\left(\frac{k_p}{k_f}-\frac{k_{nl}}{k_f}\right)\phi k_{nl}\left(2\left(1+\frac{dnl}{r_p}\right)^3-\left(1+\frac{2dnl}{r_p}\right)^3+1\right)+\left(\frac{k_p}{k_f}+2\frac{k_{nl}}{k_f}\right)\left(1+\frac{dnl}{r_p}\right)^3\left(\phi\left(1+\frac{2dnl}{r_p}\right)^3\left(\frac{k_{nl}}{k_f}-1\right)+1\right)}{\left[\left(1+\frac{dnl}{r_p}\right)^3\left(\frac{k_p}{k_f}+2\frac{k_{nl}}{k_f}\right)-\left(\frac{k_p}{k_f}-\frac{k_{nl}}{k_f}\right)\phi\left(\left(1+\frac{dnl}{r_p}\right)^3+\left(1+\frac{2dnl}{r_p}\right)^3-1\right)\right]}\left(R^2(z)-\frac{1}{2}\right)\Bigg)\Bigg]\Bigg] \tag{100}$$

Equation (49) is found applying conditions (54) and (59) to get

$$c_m=\frac{1}{2Pe\sqrt{\pi T}}\exp\left(\Lambda-\frac{z_1^2}{4T}\right) \tag{101}$$

where,

$$\Lambda(\mathrm{t})=\int_0^t K_0(\eta)d\eta \tag{102}$$

$$z_1(t,z)=z+\int_0^t K_1(\eta)d\eta \tag{103}$$

$$T(t)=\int_0^t K_2(\eta)d\eta \tag{104}$$

Since steady state is under examination, approximately Equations (94) to (96) for large time is

$$\Lambda(\mathrm{t})\sim K_0 t \tag{105}$$

$$z_1(t,z)\sim z+K_1 t \tag{106}$$

$$T(t)\sim K_2 t \tag{107}$$

4. Graphical Results and Discussions

Nano biosensors find great use in medical applications like detection of tumours and plaques. Nano biosensors have an advantage of high sensitivity because they can decipher small changes in biological element for sensing (Lee and Kim, 2024). Thus, to mathematically explore its applications, this paper studies the dispersion of nano biosensors in an artery with multiple stenosis. Nano biosensors in the form of carbon nanotubes with a coating of nanolayer is dispersed in the stenosed artery. Temperature provides a stimulus for the detection of stenosis. The nanolayer on the carbon nanotube detects the diseased site.

For the analysis of the phenomenon, graphs have been plotted for temperature as well as velocity of nano biosensors in blood against radial direction. Further, the transport coefficients of nano biosensors in blood have also been plotted against wall absorption parameter to study the dispersion. **Figures 2-13** show these variations that have been plotted in MATLAB. The values of thermophysical parameters used for calculation are given in **Table 2** in appendix.

Figure 2 is a graph displaying the temperature (θ) of nanobiosensors in the blood as a function of radial position (r), with the heat source parameter (h) acting as variable. Substantially, the heat source parameter has a central part in regulating the thermal performance of nanobiosensors, with its value affected by features such as the temperature of adjacent tissues (e.g., diseased arteries) and the thermal conductivity of blood. This constraint directly influences the nanobiosensors' thermal response, which is crucial for their functionality in numerous biomedical uses (Raza et al., 2024). The graph shows that as the heat source parameter rises, the temperature of the nanobiosensors increases too. This trend has physical significance because it advocates on regulating the heat source parameter can control the thermal environment near the sensors. Such regulation is mainly valuable in thermal-responsive path-tracing procedures, where the nanobiosensors' movement is traced based on temperature differences. By regulating the heat source parameter, researchers can affect the trajectory and performance of nanobiosensors in the bloodstream, delivering an influential means for precision tracking and supervision. This ability is particularly imperative in applications like targeted drug delivery, where knowing the precise position and movement of nanobiosensors can advance therapeutic exactness. Earlier studies by Hussain et al. (2023, 2024) have also testified to comparable findings, accentuating the important role of the heat source parameter in the nanobiosensor dynamics. Inclusively, understanding the thermal properties administered by this parameter improves the probability for improving nano biosensor-based knowhows in medical treatments.

Figure 3 shows a graph portraying the temperature (θ) of nanobiosensors in blood across the radial direction (r) for changing values of nanolayer thickness (dnl). These nanobiosensors are covered with a nanolayer for detection and signal transfer, hence the properties of this nanolayer play a decisive role in defining the efficacy of nanobiosensor perception skills. The graph divulges a clear tendency: as the thickness of the nanolayer growths, the temperature also increases. This phenomenon can be accredited to the decrease in interparticle distance arising from a thicker nanolayer. Therefore, there is an improvement in Brownian motion amid the nanoparticles, causing an inclusive growth in temperature in the blood. It is clear from these observations that the thickness of the nanolayer must be cautiously adjusted to align with the proposed purpose of the nanobiosensors. By choosing an apt nanolayer thickness, researchers can confirm optimal sensing performance while evading possible overheating problems. This underlines the significance of reflecting nanolayer properties in the strategy and development of nanobiosensors for biomedical uses. Prior studies, by Ramya et al. (2018) and Bandyopadhyay et al. (2020) have also emphasised the role of nanolayer in defining nanobiosensor efficacy, further accentuating the consequence of this parameter in sensor design and optimization.

Figure 4 is a graph showing the velocity (u) of nanobiosensors in blood across the radial direction (r) for different nanolayer thicknesses (dnl). The nanobiosensors are coated with a nanolayer for bio-sensing uses, and the thickness of this layer differs across different uses and biological situations. A prominent trend detected in the graph is that as the nanolayer thickness growths, the velocity of the nanobiosensors declines. This phenomenon can be qualified to the weakening interparticle distance ensuing from the thicker nanolayer. Consequently, the regularity of Brownian collisions between the nanoparticles is increased, causing a total decrease in velocity in the blood. This conclusion underlines the importance of controlling the thickness of the nanolayer for greater biosensing abilities. By cautiously choosing the suitable nanolayer thickness, researchers can attain optimal velocity while guaranteeing effectual bio-sensing performance. This shows the vital role of nanolayer thickness in the design and optimization of nanobiosensors for biomedical applications, as underscored in previous studies (Ramya et al., 2018).

Figure 5 is the effect of the Darcy number (Da) on the velocity (u) of nanobiosensors in blood. The Darcy number is an essential parameter that characterizes the relative significance of a medium's permeability and its cross-sectional area of flow. In real terms, a higher Darcy number indicates a medium with superior

permeability, permitting more effectual flow of fluids. Therefore, when the Darcy number reinforces, it represents amplified permeability, the velocity of nanobiosensors in the blood also increases (El Koumy et al., 2013). This relationship holds decisive implication in many biomedical applications where nanobiosensors are applied for diagnostic or therapeutic uses. Understanding how fluctuations in the Darcy number affect nanobiosensor velocity delivers appreciable understandings into optimizing their performance in biomedical settings. By controlling the relationship between the Darcy number and nanobiosensor velocity, researchers can improve the productivity and efficacy of nanobiosensor-based technologies for biomedical applications, such as targeted drug delivery or disease diagnosis.

Figure 6 shows the variation of the velocity (u) of nanobiosensors in the blood and the slip parameter (σ). The slip parameter enumerates the difference in velocities between adjacent fluid layers in laminar flow, presenting perceptions about the fluid dynamics within bloodstream. Physically, the slip parameter governs the efficiency of nanobiosensors as they move through blood by affecting the interaction between the fluid layers and the sensors. The trend detected through the study shows that as the slip parameter rises, the velocity of the nanobiosensors reduces. This behaviour can be described by the fact that slip at the boundary between fluid layers diminishes the total shear forces within the flow. Subsequently, the reduced shear force slows down the nanobiosensors. Basically, when there is more slip (less friction between layers), the fluid's capacity to transfer momentum reduces, causing a decrease in velocity of the nanobiosensors. Understanding this relationship is necessary to optimize the functionality of nanobiosensors in biomedicine (Abdelsalam and Zaher, 2023). By taking the slip parameter into consideration, researchers can control the behaviour of nano biosensors, providing for enhanced control of their movement in the blood. This is important for applications such as targeted drug delivery, where exact control of nanobiosensor velocity significantly impacts the exactness and efficiency of treatment, or in disease monitoring, where reliable sensor performance is important for accurate diagnosis. Eventually, a deeper understanding of the slip and velocity allows the advancement of more effective biomedical technologies.

Figure 7 shows the relationship between the velocity (u) of nanobiosensors in blood and stenosis depth (δ). Stenosis depth is the measurement of narrowing or constriction in the artery, that alters the flow blood flow dynamics. As the graph depicts, an upsurge in stenosis depth causes a rise in nanobiosensor velocity. This can be elucidated by Bernoulli's principle, which states that a decrease in cross-sectional area within a fluid flow system brings about an increase in velocity. For stenosed arteries, the narrowing of the arterial lumen raises blood pressure upstream of the stenosis, increasing the blood and nanobiosensors flow through the diseased region. Understanding the stenosis depth effect on flow is needed for refining the targeting precision and efficacy of nanobiosensor-based technologies. In applications like targeted drug delivery, disease monitoring, and diagnostic imaging, these flow behaviours can influence the accuracy with which nanobiosensors reach target areas in the diseased artery. By integrating an examination of multiple stenosis geometries, researchers can develop more sophisticated approaches to optimize sensor performance in real-world biomedical circumstances.

Figure 8 depicts the relationship between the velocity (u) of nanobiosensors in blood and the Grashof number (Gr). The Grashof number is representative of the ratio of buoyant forces to viscous forces in a fluid. With the increase in Grashof number, the graph illustrates an equivalent increase in nanobiosensor velocity, which is because of the domination of buoyant forces over viscosity. In simpler terms, a greater Grashof number shows that buoyancy-driven forces are stronger in relation to viscous forces (Abdelsalam and Zaher, 2023). This implies that as Gr growths, the buoyant forces on the nanobiosensors drive them more efficiently through the blood, ensuing in a clear rise in their velocity. When buoyant forces become larger than viscosity, the nanobiosensors experience resistance to a lesser extent, letting them disperse freely in the fluid. This improved motion is predominantly used in the framework of nanobiosensors in the blood,

where regulating their course is important for biomedical usage. By regulating the environments that affect the Grashof number, such as temperature gradients or fluid properties, researchers can better regulate the velocity and trajectory of nanobiosensors, refining the accuracy. The physical validation delivered by the Grashof number is a central reason of how buoyant forces effect sensor behaviour, and this understanding can be used to fine-tune the design of nanobiosensors in medical treatments.

Figure 9 shows the variation of the transport coefficient ($-K_0$) and the wall absorption parameter (β). The transport coefficient ($-K_0$) characterises the rate of nanoparticle flux at the wall of artery, showing the effectiveness of nanobiosensors reaching the target. The observed trend in the graph shows that as the wall absorption parameter (β) increases, there is an upsurge in the transport coefficient ($-K_0$). This phenomenon can be accredited to the increasing number of nanobiosensors reaching the stenosed arterial wall because of increased absorption at the wall. This relationship between the wall absorption parameter and the transport coefficient is necessary to optimize the targeting ability of nanobiosensors to diseased site. By enhancing the wall absorption parameter, researchers can expand the effectiveness of nanobiosensors in reaching the target, eventually improving the accuracy in disease detection.

Figure 10 depicts the relationship between the transport coefficient ($-K_1$) and the wall absorption parameter (β) for various thicknesses of the nanolayer (dnl). The transport coefficient ($-K_1$) signifies the rate of convection occurring due to nanobiosensors in the bloodstream. The trend as per the graph directs that as the thickness of the nanolayer (dnl) increases, there is a decline in the transport coefficient ($-K_1$). This is because of the decrease in convections arising out of thicker nanolayer. As the nanolayer thickens, the velocity of nanobiosensors or their convections in the blood reduce, leading to a decline in the transport coefficient. Thus, the nanolayer thickness and the transport coefficient is quantified for optimization in design and performance of nanobiosensor. By following the influence of nanolayer thickness on convection, researchers can progress towards more effective approaches to control nanobiosensor trajectory in the bloodstream, eventually improving the efficiency.

Figure 11 illustrates the graph of the transport coefficient ($-K_1$) and the wall absorption parameter (β) for various stenosis depths (δ). The transport coefficient ($-K_1$) characterizes the rate of convection due to nanobiosensors movement in the blood. The trend in the graph reflects that as the stenosis depth (δ) growths, there is a corresponding rise in the transport coefficient ($-K_1$). This is because of the higher velocity of nanobiosensors in the blood as the stenosis depth rises. By considering the effect of stenosis depth on nanobiosensor transport, researchers can develop more effective tactics for monitoring nanobiosensor movement in the blood. This parameter can ultimately augment the exactness and efficiency in targeted drug delivery.

Figure 12 shows the graph of the transport coefficient ($-K_2$) and the wall absorption parameter (β) for different thicknesses of the nanolayer (dnl). The transport coefficient ($-K_2$) symbolizes the rate of convection and dispersion of nanobiosensors in the bloodstream. The detected trend in the graph designates that as the thickness of the nanolayer (dnl) growths, there is a reduction in the transport coefficient ($-K_2$). This happens because of the reduction in velocity associated with the thicker nanolayer. As the nanolayer thickness growths, the velocity of nanobiosensors reduces, impeding their flow and dispersion in the bloodstream. By reflecting upon the influence of nanolayer thickness on convection and dispersion, researchers can progress to make more effective approaches for governing nanobiosensor movement in the bloodstream. This understanding can ultimately improve the precision in drug delivery.

Figure 13 exhibits the graph of the transport coefficient ($-K_2$) and the wall absorption parameter (β) for various stenosis depths (δ). The transport coefficient ($-K_2$) measures the rate of convection and dispersion

of nanobiosensors in the bloodstream. The trend in the graph directs that as the stenosis depth (δ) rises, there is a corresponding growth in the transport coefficient ($-K_2$). This is because of enhanced convection and dispersion of nanobiosensors due to greater velocity in the blood as stenosis depth surges. By reflecting upon these multiple stenosis, one can better comprehend how stenotic depth effect nanobiosensor transport and dispersion. This is decisive for designing nanobiosensor-based biomedical devices that are augmented for real-world conditions, where the exact control of sensor motion is essential.

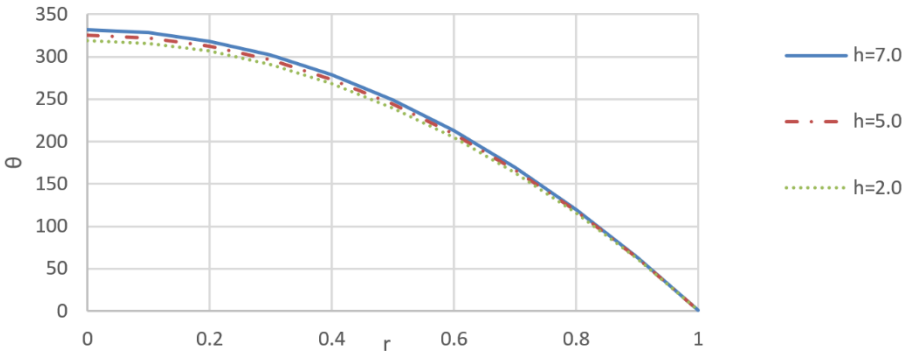

Figure 2. Graph of temperature θ of nano biosensors with radial direction r for heat source parameter h.

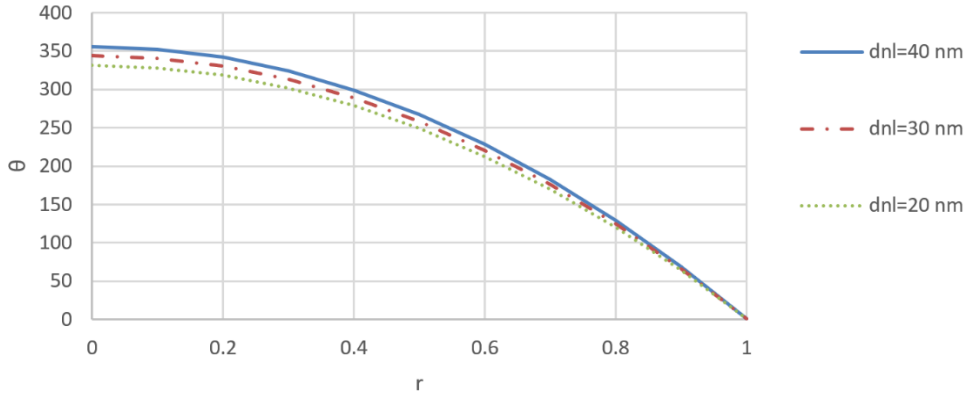

Figure 3. Graph of temperature θ of nano biosensors with radial direction r for thickness of nanolayer dnl.

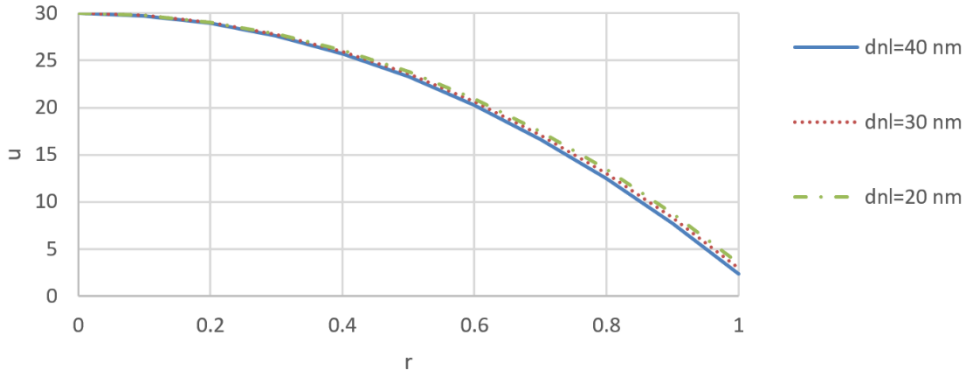

Figure 4. Graph of velocity u of nano biosensors with radial direction r for thickness of nanolayer dnl.

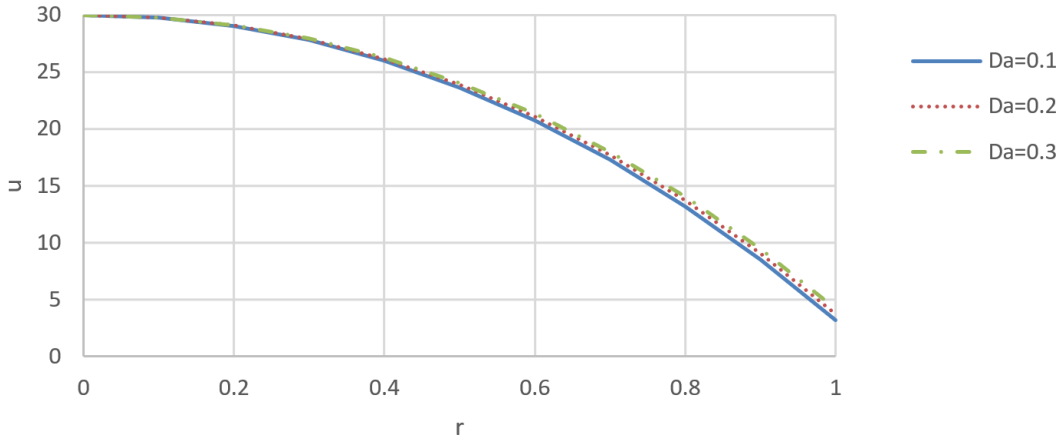

Figure 5. Graph of velocity u of nano biosensors with radial direction r for Darcy number Da.

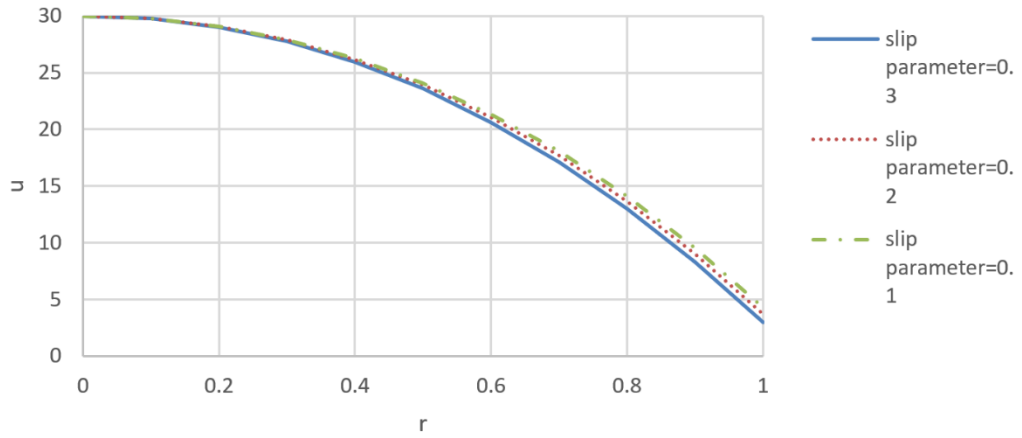

Figure 6. Graph of velocity u of nano biosensors with radial direction r for slip parameter σ.

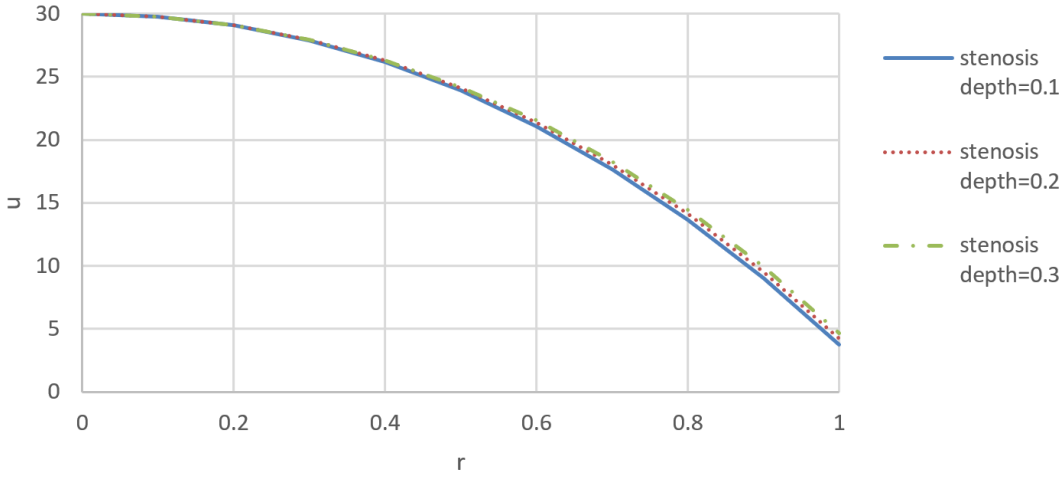

Figure 7. Graph of velocity u of nano biosensors with radial direction r for stenosis depth δ.

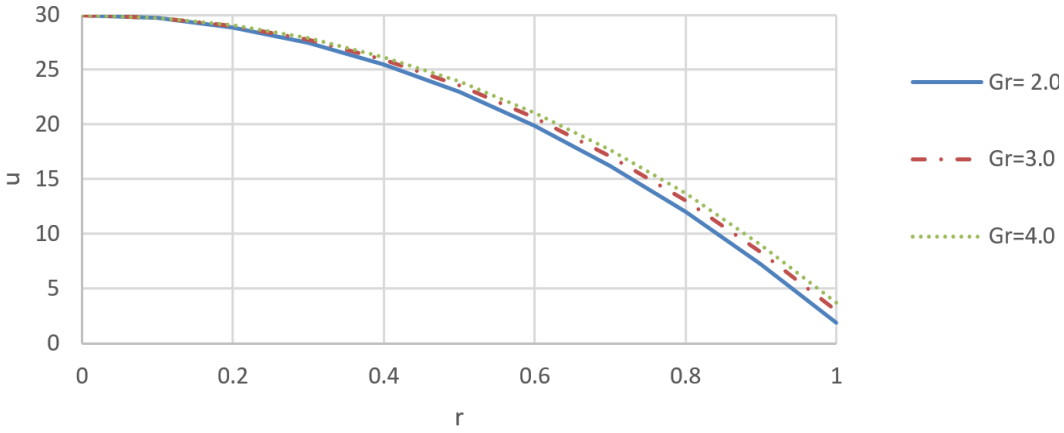

Figure 8. Graph of velocity *u* of nano biosensors with radial direction *r* for Grashof number *Gr*.

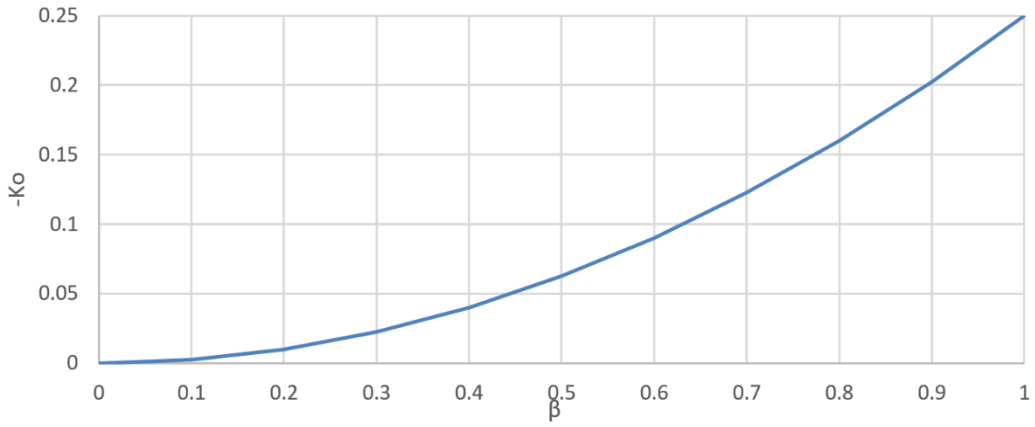

Figure 9. Graph of transport coefficient $-K_0$ of nano biosensors with wall absorption parameter β.

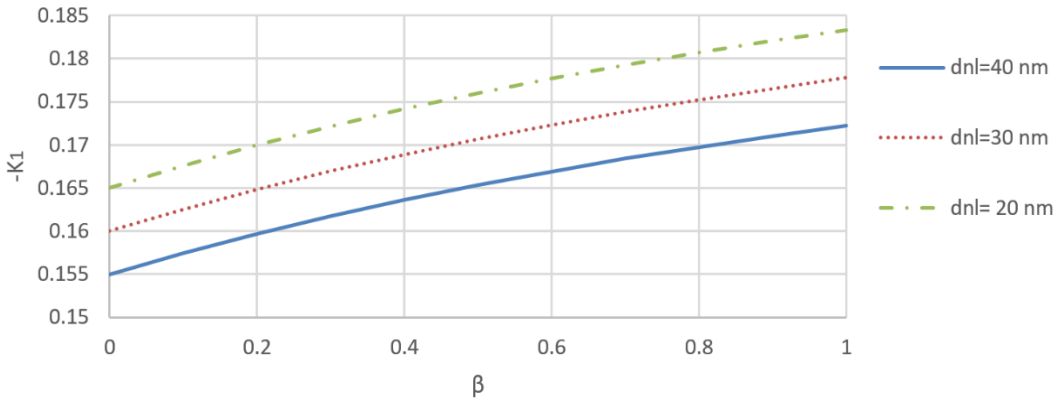

Figure 10. Graph of transport coefficient $-K_1$ of nano biosensors with wall absorption parameter β for thickness of nanolayer *dnl*.

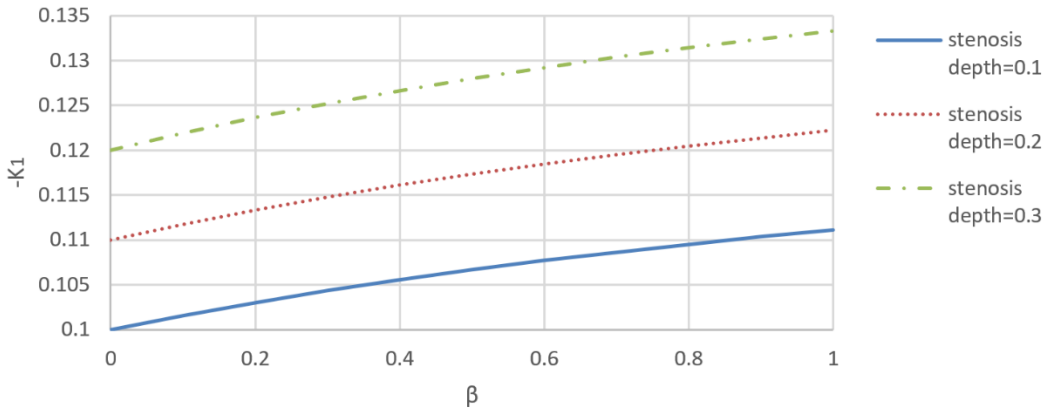

Figure 11. Graph of transport coefficient- K_1 of nano biosensors with wall absorption parameter β for thickness of nanolayer δ.

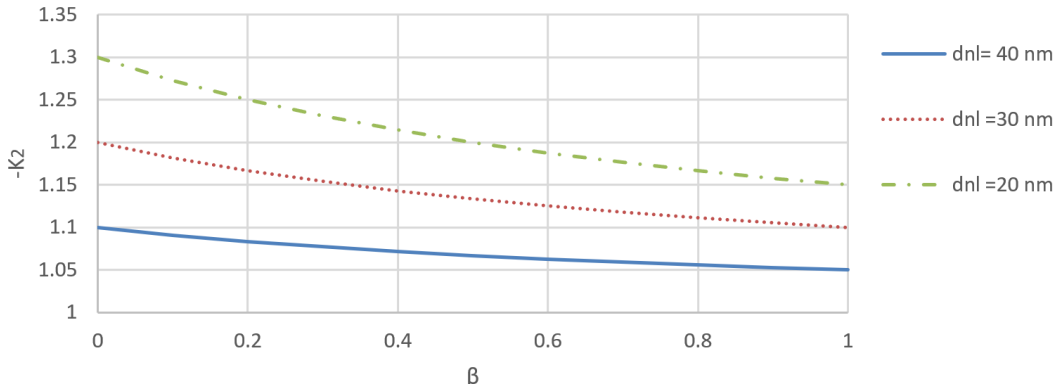

Figure 12. Graph of transport coefficient -K_2 of nano biosensors with wall absorption parameter β for thickness of nanolayer *dnl*.

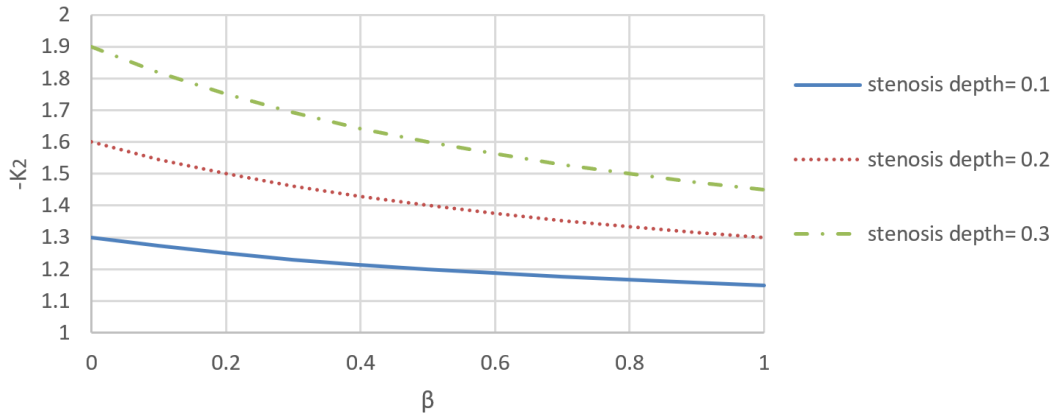

Figure 13. Graph of transport coefficient -K_2 of nano biosensors with wall absorption parameter β for stenosis depth δ.

4.1 Sensitivity Analysis

Nanobiosensors hold immense potential for targeted drug delivery and diagnostics, but their performance can be significantly affected by factors such as nanolayer thickness and stenosis depth. To better understand the impact of these parameters, we have employed sensitivity analysis using the partial differentiation method. Equations (98) and (100) were differentiated partially with respect to d_{nl} and δ to measure the fluctuations in these parameters that affect the transport coefficients K_1 and K_2, which direct the convection and dispersion of nanobiosensors in the blood. The sensitivity analysis outcomes for the transport coefficients K_1 and K_2 designate that both coefficients are significantly affected by the nanolayer thickness and stenosis depth.

(i) Effect of Nanolayer Thickness: As the nanolayer thickness growths, there is a clear reduction in the transport coefficients K_1 and K_2. This inverse relationship advocates that a thicker nanolayer causes a larger resistant to the motion of nanobiosensors, thus reducing the total effectiveness of their dispersion in the blood. The declined movement is possibly due to the amplified interaction between the nanolayer and the flow, impeding the convection and diffusion progressions.

(ii) Effect of Stenosis Depth: In contrast, both K_1 and K_2 display a positive association with stenosis depth. As the stenosis depth surges, there is a surge in the values of K_1 and K_2. This behaviour is due to the narrowing of the arterial lumen, which quickens flow of blood, improving the convection and dispersion of nanobiosensors. The improved velocity in the stenosed regions assists in transporting the biosensors more effectually, leading to greater values of the transport coefficients.

5. Conclusion

Nanotechnology has notably progressed biosensing technology by presenting improved abilities of different nanomaterials such as metal nanoparticles, nanotubes, nanorods, and nanowires. These nanomaterials offer an outstanding platform to diagnose cardiovascular diseases.

This research explores the features of nano-biosensors dispersed in a diseased artery with multiple stenoses. Nano-biosensors have substantial physical significance due to their capability to perceive precise biological signals and respond to biological fluctuations in real-time. They can cross the intricate vascular environment and interact with biological tissues on a nanoscale level, thus making them perfect for targeted diagnostics, disease monitoring, and drug delivery. Specifically, this study inspects the effect of nanolayer thickness on nano-biosensor behaviour upon temperature stimulation. The model is developed using the equation of continuity, Navier-Stokes equation (or equation of motion), and the diffusion equation. The mathematical model is solved analytically, and graphs of temperature, velocity, and transport coefficients are plotted using MATLAB.

The physical implication of nano-biosensors lies in their capacity of responding to confined or local environments within the bloodstream, such as temperature deviations, pressure gradients, or chemical signals. This permits them to perform exact functions, like perceiving inflammation or releasing drugs at the target sites or diseased site.

The mathematical consequences of this study can be recapitulated as:
(1) Temperature: The temperature of nano-biosensors rises with a rise in the heat source parameter and the thickness of the nanolayer. This advocates that factors such as heat needed to trigger the nanobiosensors and thicker nanolayers influence the thermal response of nano-biosensors.

(2) Velocity: The velocity rises with greater Grashof and Darcy numbers, while it declines with increasing nanolayer thickness, slip parameter, and stenosis depth. This illustrates that fluid flow dynamics and arterial conditions strongly effect the motion and dispersion of nano-biosensors.

(3) Transport Coefficients: The transport coefficients K_0 and K_1 surge with the wall absorption parameter, while K_2 declines. This signifies that a greater interaction between the biosensors and the arterial wall improves nanoparticle transport while reducing dispersion, which is applicable for targeted drug delivery.

(4) Nanolayer and Stenosis Impact: Both K_1 and K_2 rise with diminishing nanolayer thickness and growing stenosis depth. This shows the significance of nanolayer properties and arterial conditions in regulating biosensor motion.

(5) For stenosis depths extending from $0.1x10^{(-3)}$ m to $0.3x10^{(-3)}$ m, nano-biosensors bearing a layer thickness of 30 nm shall be optimal in the temperature range of 310K-320K.

Although the conclusions are promising, it is significant to recognize some limitations and challenges intrinsic to the modelling process. For instance, the complex geometry of arteries having multiple stenoses presents possible uncertainties in the dispersion of nano-biosensors. These probabilities may be reflected upon in further investigations when interpreting the study's consequences and applying them to biomedical practices.

To sum up, this research offers a strong groundwork for the development nano-biosensors to treat, diagnose and manage cardiovascular disease. Incorporating the study's considerations shall allow the development of more robust, dependable, and clinically feasible biosensing technologies. Further investigation of nanobiosensor sensitivity and stimuli response will also help expand their functionality in dynamic biological environments, improving their possibility for effective incorporation into biomedical systems, practices and treatment strategies.

Conflict of Interest
The authors confirm that there is no conflict of interest to declare for this publication.

AI Disclosure
The author(s) declare that no assistance is taken from generative AI to write this article.

Acknowledgments
This research did not receive any specific grant from funding agencies in the public, commercial, or not-for-profit sectors. The author would like to thank the editor and anonymous reviewers for their comments that help improve the quality of this work.

Appendix

Table 1. List of symbols.

Symbol	Meaning
r'	Dimensional radial direction
θ'	Dimensional azimuthal direction
z'	Dimensional axial direction
$R'(z')$	Dimensional radius of artery
R_0	Radius of non-stenosed artery
δ_i'	Dimensional stenosis depth

Table 1 continued…

d_i'	Dimensional stenosis location
S_i'	Dimensional stenosis width
L'	Dimensional length of arterial section
ρ_{nf}	Density of nanofluid
u'	Dimensional axial velocity
v'	Dimensional radial velocity
w'	Dimensional azimuthal velocity
t'	Dimensional time
$F_{r'}, F_{\theta'}, F_{z'}$	Dimensional body forces in respective directions
P'	Dimensional pressure
D_{nf}	Thermal diffusivity of nanofluid
T'	Dimensional temperature
H	Heat source parameter
k_{nf}	Thermal conductivity of nanofluid
c'	Dimensional concentration of nanobiosensors
D'	Dimensional diffusivity of nanobiosensors
m'	Rate at which nanoparticles are released or absorbed
d_{nl}	Thickness of nanolayer (on biosensors)
k_f	Thermal conductivity of blood
k_p	Thermal conductivity of nanobiosensor
k_{nl}	Thermal conductivity of nanolayer
r_p	Radius of nanobiosensor
ϕ	Volume fraction of nanobiosensor
μ_{nf}	Viscosity of nanofluid
μ_f	Viscosity of blood
A_1, A_2	Shape parameter of nanoparticle
$\rho\gamma_{nf}$	Thermal expansion of nanofluid
$\rho\gamma_f$	Thermal expansion of blood
$\rho\gamma_p$	Thermal expansion of nanobiosensor
g	Acceleration due to gravity
u_B'	Dimensional velocity of slip
u_p'	Dimensional velocity at the arterial boundary
σ'	Dimensional slip parameter
k_o'	Dimensional permeability at the arterial boundary
T_o	Temperature on the surface of the artery
Da	Darcy number
Gr	Grashof number
Pe	Peclet number
u_{avg}	Reference velocity
c_α	Reference concentration
β	Wall absorption parameter
θ	Non- dimensional temperature
u	Non- dimensional axial velocity
K_0, K_1, K_2	Transport coefficients

The symbols without dash represent non-dimensional quantities.

Table 2. Thermophysical values for properties of blood and carbon nanotubes used for calculations.

Physical properties	**Blood (Bali and Prasad, 2022)**	**Carbon nanotubes (Ferrier and Honeychurch, 2021)**
Heat Capacitance (c_p)	3594 J/Kg K	550 J/Kg K
Thermal Conductivity (k)	0.492W/m_ K	3000 W/m K
Density (ρ)	1060 Kg/m^3	1300 Kg/m^3
Thermal expansion coefficient (γ)	0.18 X 10^{-5} K^{-1}	2.1 X 10^{-5} K^{-1}

References

Abdelsalam, S.I., & Zaher, A.Z. (2023). Biomimetic amelioration of zirconium nanoparticles on a rigid substrate over viscous slime- a physiological approach. *Applied Mathematics and Mechanics*, *44*(09), 1563-1576. https://doi.org/10.1007/s10483-023-3030-7.

Abdelsalam, S.I., Abbas, W., Megahed, A.M., & Said, A.A.M. (2023). A comparative study on the rheological properties of upper convected Maxwell fluid along a permeable stretched sheet. *Helion, 09*(12), e22740. https://doi.org/10.1016/j.heliyon.2023.e22740.

Abdelsalam, S.I., Abdelwahab, E.T., Eldesoky, I.M., Abumandour, R.M., & Ahmed, M.M. (2024a). Benchmarking the composite performance of distinct shapes of ferro metallic gold nano shells: photo thermal cancer therapy. *Acta Mechanical Sinica, 41,* 724077. https://doi.org/10.1007/s10409-024-24077-x.

Abdelsalam, S.I., Magesh, A., & Tamizharasi, D. (2024b) Optimizing fluid dynamics: an in-depth study for nano-biomedical applications with a heat source. *Journal of Thermal Analysis and Calorimetry*. https://doi.org/10.1007/s10973-024-13472-2. (In press).

Adhikari, R., Das, S., & Das, S. (2024). Neural networks-based framework for recognizing streaming patterns in magnetized Maxwell-Oldroyd-B blood blended with tetra-hybrid nanoparticles and microbes over stenosis in an elastic artery. *Engineering Applications of Artificial Intelligence, 136*(part B), 109048. https://doi.org/10.1016/j.engappai.2024.109048.

Alhussain, Z.A. (2022). Comprehensive study of thermal conductivity models with metallic and non-metallic nanoparticles in the blood flow through a regular catheter in a multi-stenosed artery. *Applied Nanoscience*, *12*(12), 4033-4045. https://doi.org/10.1007/s13204-022-02622-3.

Arndt, N., Tran, H.D.N., Zhang, R., Xu, Z.P., & Ta, H.T. (2020). Different approaches to develop nano sensors for diagnosis of diseases. *Advanced Science*, *7*(24), 2001476. https://doi.org/10.1002/advs.202001476.

Bali, R., & Prasad, B. (2022). Study of effect of various shapes of nanoparticles in catheterized artery with elliptical stenosis: comparing analytical and numerical solution. *Ganita, 72*(02), 127-151.

Bandyopadhyay, S., Shao, L., Wang, C., Liu, S., Wu, Q., Gu, G., Hu, J., Liu, Y., Chen, X., Song, Z., Song, X., Bao, Q., & Smietana, M. (2020). Study on optimization of nano-coatings for ultra-sensitive biosensors based on long-period fibre grating. *Sensing and Bio-Sensing Research*, *27*, 100320. https://doi.org/10.1016/j.sbsr.2019.100320.

Batchelor, G.K. (1977). The effect of Brownian motion on the bulk stress in a suspension of spherical particles. *Journal of Fluid Mechanics*, *83*(1), 97-117. https://doi.org/10.1017/s0022112077001062.

El Koumy, R.S., Barakat, E.S.I., & Abdelsalam, S.I. (2013). Hall and transverse magnetic field effects on peristaltic flow of a Maxwell fluid through a porous medium. *Global Journal of Pure and Applied Mathematics, 09*(02), 187-203. https://www.ripublication.com/gjpam.htm.

Ferrier, D.C., & Honeychurch, K.C. (2021). Carbon nanotube (CNT)-based biosensors. *Biosensors*, *11*(12), 486. https://doi.org/10.3390/bios11120486.

Gergeroglu, H., Yildirim, S., & Ebeoglugil, M.F. (2020). Nano-carbons in biosensor applications: an overview of carbon nanotubes (CNTs) and fullerenes (C60). *SN Applied Sciences*, *2*, 603. https://doi.org/10.1007/s42452-020-2404-1.

Huang, X., Zhu, Y., & Kianfar, E. (2021). Nano biosensors: properties, applications and electrochemical techniques. *Journal of Materials Research and Technology*, *12*, 1649-1672. https://doi.org/10.1016/j.jmrt.2021.03.048.

Hussain, A., Dar, M.N.R., Cheema, W.K., Han, Y., & Kanwal, R. (2023). Clinical symbiosis of hybrid nanoparticles and induced magnetic field on heat and mass transfer in multiple stenosed artery with erratic thrombosis. *Scientific Reports*, *13*, 15588. https://doi.org/10.1038/s41598-023-42795-7.

Hussain, A., Dar, M.N.R., Cheema, W.K., Kanwal, R., & Han, Y. (2024). Investigating hybrid nanoparticles for drug delivery in multi-stenosed catheterized arteries under magnetic field effects. *Scientific Reports*, *14*, 1170. https://doi.org/10.1038/s41598-024-51607-5.

Karmakar, P., & Das, S. (2023). Modelling non-Newtonian magnetized blood circulation with tri-nanoadditives in a charged artery. *Journal of Computational Science*, *70,* 10203. https://doi.org/10.1016/j.jocs.2023.102031.

Kiran, M., & Mahesh, G. (2016). Nano sensors success in cardiovascular diseases. *Research and Reviews: Journal of Pharmaceutics and Nanotechnology*, *4*(2), 1-7.

Kulkarni, M.B., Ayachit, N.H., & Aminabhavi, T.M. (2022). Recent advancements in nanobiosensors: current trends, challenges, applications, and future scope. *Biosensors*, *12*(10), 892. https://doi.org/10.3390/bios12100892.

Kumar, P.P., Balakrishnan, S., Magesh, A., Tamizzharasi, P. & Abdelsalam, S.I. (2024). Numerical treatment of entropy generation and Bejan number into an electro osmotically- driven flow of Sutterby nanofluid in an asymmetric microchannel. *Numerical Heat Transfer, Part B: Fundamentals*, 1-20. https://doi.org/10.1080/10407790.2024.2329773.

Lee, J.H., & Kim, K.S. (2024). Nano/micro biosensors for biomedical applications. *Biosensors*, *14*(2), 58. https://doi.org/10.3390/bios14020058.

Malik, P., Katyal, V., Malik, V., Asatkar, A., Inwati, G., & Mukherjee, T.K. (2013). Nano biosensors: concepts and variations. *ISRN Nanomaterials, 2013*(327435), 1-9. https://doi.org/10.1155/2013/327435.

Malik, S., Singh, J., Goyat, R., Saharan, Y., Chaudhry, V., Umar, A., Ibrahim, A.A., Akbar, S., Ameen, S., & Baskoutas, S. (2023). Nanomaterials-based biosensor and their applications: a review. *Helion, 9*(9), e19929. https://doi.org/10.1016/j.heliyon.2023.e19929.

Murshed, S.M.S., Leong, K.C., & Yang, C. (2008). Investigations of thermal conductivity and viscosity of nanofluids. *International Journal of Thermal Science, 47*(5), 560-568. https://doi.org/10.1016/j.ijthermalsci.2007.05.004.

Muthtamilselvan, M., & Gifteena Hingis, Y.M. (2022). Theoretical study of gold nanoparticles and microorganisms in the blood flow of a regular catheterized multi-stenosed artery. *Research Article Preprint*. https://doi.org/10.21203/rs.3.rs-1801992/v1.

Naresh, V., & Lee, N. (2021). A review on biosensors and recent development of nanostructured materials-enabled biosensors. *Sensors*, *21*(4), 1109. https://doi.org/10.3390/s21041109.

Philip, J.R. (1957). Numerical solution of the diffusion type with diffusivity concentration? Dependent II. *Australian Journal of Physics, 10*(1), 29-42. https://doi.org/10.1071/ph570029.

Qiu, L., Zhu, N., Feng, Y., Michaelides, E.E., Zyla, G., Jing, D., Zhang, X., Norris, P.M., Markides, C.N., & Mahian, O. (2020). A review of recent advances in thermophysical properties at the nanoscale: from solid state to colloids. *Physics Reports*, *843*, 1-81. https://doi.org/10.1016/j.physrep.2019.12.001.

Raju, C.S.K., Basha, H.T., Noor, N.F.M., Shah, N.A., & Yook, S.J. (2024). Significance of body acceleration and gold nanoparticles through blood flow in an uneven stenosis artery: a finite difference computation. *Mathematics and Computers in Simulation, 215*, 399-419. https://doi.org/10.1016/j.matcom.2023.08.006.

Ramesh, M., Janani, R., Deepa, C., & Rajeshkumar, L. (2023). Nanotechnology-enabled biosensors: a review of fundamentals, design principles, materials, and applications. *Biosensors*, *13*(1), 40. https://doi.org/10.3390/bios13010040.

Ramya, D., Raju, R.S., Rao, J.A., & Chamkha, A.J. (2018). Effects of velocity and thermal wall slip on magnetohydrodynamics boundary layer viscous flow and heat transfer of a nanofluid over a non-linearly-stretching sheet: a numerical study. *Propulsion and Power Research*, *7*(2), 182-195. https://doi.org/10.1016/j.ppr.2018.04.003.

Raza, R., Naz, R., Murtaza, S., & Abdelsalam, S.I. (2024). Novel nanostructural features of heat and mass transfer of radioactive Carreau nano liquid above an extendable rotating disk. *International Journal of Modern Physics B*, *38*(30), 2450407. https://doi.org/10.1142/s0217979224504071.

Sagadevan, S., & Periasamy, M. (2014). Recent trends in nanobiosensors and their applications - a review. *Reviews in Advanced Material Science*, *36*, 62-69.

Sankarsubramanian, R., & Gill, W.N. (1973). Unsteady convective diffusion with interphase mass transfer. *Proceedings of The Royal Society A*, *333*(1592), 115-132. https://doi.org/10.1098/rspa.1973.0051.

Sayah, R.M., Ebrahimi, S., Mirafzal, I. & Shamloo, A. (2024). Investigation of the size and shape of nanomicrocarriers for targeted drug delivery to atherosclerotic plaque in ischemic stroke prevention. *International Journal of Pharmaceutics*, *662,* 124469. https://doi.prg/10.1016/j.ijpharm.2024.124469.

Shah, S. (2009). Numerical simulation of particle adhesion dynamics for applications in nanomedicine and biosensing. UTA, *Medicine, Engineering, Material Science*. https://api.semanticscholar.org/CorpusID:139599682.

Shamloo, A., Naseri, T., Rahbary, A., Bakhitari, M.A., Ebrahimi, S., & Mirafzal, I. (2023). In-silico study of drug delivery to atherosclerosis in the human carotid artery using metal-organic frameworks based on adhesion of nanocarriers. *Scientific Reports*, *13,* 21481. https://doi.org/10.1038/s41598-023-48803-0.

Shobha, B.N., & Muniraj, N.J.R. (2012). Mathematical modelling and analysis of nano biosensors for automated disease detection and drug delivery system. *International Journal of Recent Technology and Engineering*, *1*(4), 14-19.

Singh, N., Dkhar, D.S., Chandra, P., & Azad, U.P. (2023). Nano biosensors design using 2 D materials: implementation in infections and fatal disease diagnosis. *Biosensors*, *13*(2), 166. https://doi.org/10.3390/bios13020166.

Singh, S., & Melnik, R. (2022). Coupled multiphysics modelling of sensors for chemical, biomedical, and environmental applications with focus on smart materials and low dimensional nanostructures. *Chemosensors*, *10*(5), 157. https://doi.org/10.3390/chemosensors10050157.

Tîlmaciu, C.M., & Morris, M.C. (2015). Carbon nanotube biosensors. *Frontiers in Chemistry*, *3*(59), 1-21. https://doi.org/10.3389/fchem.2015.00059.

World Heart Federation. (2023). World heart report 2023: confronting the world's number one killer. Geneva, Switzerland: World Heart Federation.